Real Ambient Particulate Matter-Induced Myocardial Hypertrophy and Myocardial Lipotoxicity : Roles of PDGFRβ Methylation

Ying Zhang
Qingdao University Medical College
Xinyun Dun
Qingdao University Medical College
Benying Li
Qingdao University Medical College
Hongxu Bao
Qingdao University
Danchuan Li
Sun Yat-Sen University
Zijian Xu
Qingdao University Medical College
Angdong Ji
Qingdao University Medical College
Zhenzhen Jin
Columbia University
Jianxun Wang
Qingdao University Medical College
Rong Zhang
Hebei Medical University
Rui Chen
Capital Medical University
Wen Chen
Sun Yat-Sen University
Yuxin Zheng
Qingdao University Medical College
Lianhua Cui (qdlhcui@qdu.edu.cn)
Qingdao University Medical College

Research

Keywords: RRBS, PM, PDGFRβ, Lipid metabolism, Cardiac hypertrophy

Posted Date: December 3rd, 2021

DOI: https://doi.org/10.21203/rs.3.rs-1125976/v1

Abstract

Background: PM exposure can lead to myocardial hypertrophy, with a potential contribution via DNA methylation. Myocardial lipotoxicity is closely related to myocardial hypertrophy. But, myocardial lipotoxicity caused by PM has not been reported. PDGFRβ, a platelet-derived growth factor receptor, is also essential for normal cardiovascular development. However, It is unclear the role of PM-induced PDGFRβ methylation in myocardial hypertrophy and myocardial lipotoxicity. We investigated the effect of PDGFRβ methylation induced by PM on myocardial hypertrophy and myocardial lipotoxicity.

Results: PDGFRβ methylation caused by PM decreased PDGFRβ mRNA and protein expression in C57BL/6J mouse hearts. Thus inhibiting gene expression in its downstream pathway, ultimately leading to cardiac hypertrophy. Disturbances of myocardial lipid metabolism caused by PM in AC16 cells and C57BL/6J mouse hearts were also observed. High expression of PDGFRβ in neonatal rat primary cardiomyocytes was found to activate its downstream pathway and ameliorate the effects of PM-induced cardiac hypertrophic activity. At the same time, adenovirus was used to induce high expression of PDGFRβ in C57BL/6J mice. It was found that PDGFRβ not only improved PM-induced cardiac hypertrophy, but also alleviated PM-induced myocardial lipotoxicity.

Conclusions: PDGFRβ gene methylation may be one of the potential biomarkers of myocardial hypertrophy induced by PM exposure. And high expression of PDGFRβ may be a potential way to prevent myocardial hypertrophy and cardiac lipid metabolism disorder caused by PM exposure in mice.

Background

The relationship between environmental particulate matter (PM) pollution and the risk of cardiovascular disease (CVD) [1-3] is well established. For example, environmental PM concentration is associated with a variety of clinical manifestations of cardiovascular disease, including myocardial infarction, stroke, heart failure, arrhythmia, and venous thromboembolism [4]. Cardiac hypertrophy is a common pathology of many cardiovascular diseases, characterized by increased cell size and protein synthesis, which ultimately leads to reduced cardiac contractility and changes in coronary artery perfusion [5]. Studies have also demonstrated that PM exposure can result in fluctuant cardiac hypertrophic effects [6]. Our previous studies demonstrated that PM exposure could lead to an increase in the thickness of the right ventricular free wall in mice, resulting in a phenotype resembling cardiac hypertrophy [7-9].

Whilst prior work has implicated DNA methylation in PM induced cardiotoxicity [10, 11], the specifics of this mechanism are still unclear. Cardiac hypertrophy involves embryonic gene expression and transcriptional reprogramming, which are strictly regulated by epigenetic mechanisms. The role of DNA methylation is increasingly accepted to play an important role in the occurrence and development of cardiac hypertrophy [12].

DNA methylation can either positively or negatively regulate cardiac hypertrophy [13]. However, the development of myocardial hypertrophy requires profound changes in myocardial metabolism,

characterized by the transformation from fatty acid utilization to glycolysis and lipid accumulation. Lipids represent not only important components of the cell membrane and a critical energy source, but are also essential in cell development, differentiation and apoptosis [14-16]. Abnormal lipid metabolism is closely related to the occurrence and development of many diseases [17, 18]. Peroxisomal proliferator-activated receptor-α (PPARα) and peroxisomal proliferator-activated receptor -γ (PPARγ) play a key role in synergistic regulation of cardiac lipid metabolism through transcriptional control [19, 20]. Based upon this evidence, we assumed that PM exposure might result in myocardial lipotoxicity through the DNA methylation induced by PM exposure.

The platelet-derived growth factor (PDGF) family is a group of multifunctional proteins which stimulate angiogenesis through promoting cell proliferation and differentiation. PDGFs exert their biological activity by activating two structurally related tyrosine kinase receptors, Platelet-dervied growth factor α (PDGFRα) and platelet-dervied growth factor β (PDGFRβ) [21]. PDGFRβ, a platelet-derived growth factor receptor, is essential for the normal development of the cardiovascular system and helps rearrange the actin cytoskeleton. The role of PDGFRβ signaling in angiogenesis and early hematopoiesis has been established [22]. In addition, inactivation of PDGFRβ signaling can lead to cardiac abnormalities, including ventricular septal defect, late-embryonic ventricular dilatation, coronary vascular smooth muscle cell deficiency, and myocardial trabecular formation [23-26]. We hypothesized that PDGFRβ methylation induced by PM exposure plays an essential role in cardiac hypertrophy and cardiac lipotoxicity.

Methods

1. Individual ventilated cage (IVC)-based real-ambient PM exposure system

The real-ambient PM exposure system was used to expose mice to PM in Shijiazhuang city, Hebei Province. See Li et al for the working principle of the system [27]. Seven-week old C57/B6 male mice were purchased from Lukang Phar-maceutical (Jining, China). The C57/B6 male mice were exposed to PM for 16 hours a day (7 am 11 PM) and divided into two groups (control group and PM exposure group), each group of 30, which were exposed to PM in the air filter control room and PM exposure room respectively, for 6 consecutive weeks.

2. PM preparation

Two High-Volume Air Samples (Thermo Fischer Scientific, Waltham, MA, USA) were installed on the roof of an eight-story building located at School of Public Health, Hebei Medical University, which was about 10 m in vertical distance from the inlet of the PM exposure system. The PM2.5 was collected on Teflon or quartz filters for 24 h a day for three consecutive months from November 10, 2017, to February 1, 2018, at a flow rate of 1.05 L/min. The collected film was cut into 1x1cm size and placed into a conical flask filled with ultra-pure water. The film was ultrasonized at 80W for 30min at 20℃.Then it is placed in a thermostatic oscillator with a speed of 150 for 20min and about 20℃.Repeat the above steps three

times. The collected liquid is filtered and then put into a vacuum freeze dryer (CREATRUST, China) to dry. The collected PM particles were stored at -80℃. Our previous research analyzed the composition of particulate matter [11].

3. Adenoviral infection and tracheal drip.

Six-week old C57/B6 male mice were purchased from SPF (Beijing) Laboratory Animal Science and Technology Co., LTD.The animals were acclimated for 24 h and then randomly divided into control group, PM exposure group, hPDGFRβ-con group, hPDGFRβ-con group + PM, hPDGFRβ group, hPDGFRβ group + PM. Each group contained 8 mice. Adenovirus (AAV9) was injected into mice by tail vein injection. Administration of 1 × 1011 genome copies per mouse. 20 days after gene overexpression, let's get a tracheal drip. Tracheal drip was administered once a week for four weeks. PM was exposed by cold light source and tracheal drip. PM suspension was prepared with normal saline, and PM suspension was dropped into each exposed group at a dose of 2.7mg/kg. Fixation and infusion were completed within two minutes after anesthesia. The PM exposure dose of mice was calculated by the following formula and was consistent with the real-ambient PM exposure system. The PM exposure dose was calculated based on the average daily PM concentration of 68μg/m3 [11] in the real-ambient PM exposure system and the physiological parameters of mice. For example, 25g mice had a respiratory rate of about 163 breaths per minute and a respiratory volume of about 0.15mL per breath. The daily PM exposure of a 25g mouse was calculated to be about 16 hours x 60 minutes x 0.15mL x 163 x 68μg/m3=1.60μg. PM exposure was 1.60x42 =67.2μg per mouse at day 42. So, the final exposure dose of tracheal drip was 2.7mg/kg. All the procedures used in this study have been approved by Qingdao University Animal Care and Use Committee in keeping with the National Institutes of Health guidelines.

4. Extraction of primary cardiomyocytes

The Suckling mice, 1 to 3 days old, were washed with 75% alcohol for 2-3 times and placed in a sterilized ultra-clean table for heart extraction. After washing with PBS for 3-4 times, the heart tissue was cut into pieces and digested by adding digestive solution, which was made up of type Ⅱcollagenase (Sigma, USA), pancreatin (Sigma, USA) and PBS. After 6-7 times of digestion, the tissue mass is almost gone. Centrifuge, discard the supernatant and collect the precipitate. After fully resuspended with cell medium, the cells were filtered through a 260-mesh filter. After the collected liquid was placed in a 10cm plate, it was placed in a cell culture incubator for differential attachment for 1.5h, and then the cell suspension was collected, centrifuged, and the supernatant was discarded to obtain cardiomyocytes.

5. Cell culture

Wuhan servicebio technology CO.,LTD provided the human cardiomyocytes AC16 cell line. AC16 cells were grown in DMEM high sugar (Biosharp, China), containing 10% fetal bovine serum (FBS) (Excell, South America), 100 mg/mL streptomyocycin and 100 U/mL penicillin (Solarbio, China). Primary neonatal cardiomyocyte cells were grown in DMEM/F12(1:1) (Biosharp, China), containing 5% fetal bovine serum (FBS) (Excell, South America), 100 mg/mL streptomyocycin and 100 U/mL penicillin

(Solarbio, China). Both cells were placed in an incubator containing 95% air and 5% carbon dioxide at 37℃. Cells were seeded in 6-well plates (96-well for CCK8 assay) at the density of 1x106 cells/mL or 1x105 cells/mL. The cells grew adherently need 24 h. Then, cardiomyocytes were treated with PM2.5 samples at a concentration of (25,50,100,200 μg/mL) for 24h. Before exposure to cells, PM2.5 dissolved in DMSO (Solarbio, China) was subjected to ultrasonic treatment for 15min, while DMEM/F12(1:1) containing the same volume of DMSO was used in the control group. In experiments treated with methylation inhibitors (5AZA), cardiomyocytes were pretreated with 5AZA for 24h before exposure to PM2.5.

6. Western blotting analysis

The protein expression levels of RAS, RAF, MEK, ERK, pMEK, pERK, PDGFRβ were detected by western blot to analyze impact of PM2.5, hPDGFRβ, 5aza on primary neonatal cardiomyocyte cells. A kit for protein extraction (Solarbio, China) was performed to extract the total protein extraction in myocardial cells and myocardial tissue, and the BCA protein assay (Yeasen, China) was used to measure the concentration of the total protein. The same amounts of lysate proteins (20 mg in primary neonatal cardiomyocyte cells and 50 mg in cardiac tissue) were loaded onto SDS-polyacrylamide gels (10% separation gels). The PVDF membrane then were blocked in phosphate buffer saline (PBS) contained 5% nonfat milk for 2 h, and the PVDF membrane was incubated with the primary antibody (ABclonal, China) at 4℃ overnight, washed with PBST three times for 10 min each time, and incubated with anti-rabbit and anti-mouse Ig G secondary antibody (ABclonal, China) at room temperature for 2 h. Then we washed the PVDF membrane three time (10 min each) with PBST. At last, the antibody-bound proteins were detected by the Omni-ECLTM chemiluminescence reagent (EpiZyme, China). GAPDH was used as loading controls for the total protein content.

7. Reverse transcription quantitative polymerase chain reaction (RT-qPCR)

RNA was extracted from the frozen heart tissue samples and harvested cells using TRIzolTM Reagent (EpiZyme, China) according to the manufacturer's protocol. The RNA concentration of each sample was detected by NanoDrop-2000 (Thermo, USA), and the RNA was converted to cDNA through the kit (TargetMol, USA). RT-qPCR reaction was conducted using QuantStudio 7 Flex (Thermo Fisher Scientific, USA). SYBR Green from TargetMol, USA.The results were expressed as multiples of the increase or decrease of GAPDH. Primer sequences for all tested genes are listed in the table (table1). We conducted the assay in three biological repeats and three duplicated repeats.

8. Histology stainings.

After the mouse heart was removed, 4% paraformaldehyde was fixed at room temperature for at least 24h. After dehydration and transparency, the hearts were embedded and sliced into slices of 4μm thickness. H&E, Masson's trichrome staining were performed using standard procedures. Tissue oil red 0 staining was performed by freezing sectioning into 10μm slices and following standard procedures as for cell staining (Beyotime, China). For the thickness of the free wall of the right ventricle see Jiang et al [28].

9. Cell transfection for recombinant plasmid and adenovirus infection.

The cells were cultured into the 6-well plates at a dose of 4 × 105/ mL, high expression PDGFRβ(h PDGFRβ) recombinant enhanced green fluorescent protein (EGFP) and empty plasmids (Shanghai Genechem Co.,Ltd) into human primary cardiomyocytes, when the cell confluence was up to 70–80%. All the steps were conducted according to the instructions of Lipofectamine 2000 (Thermo Fisher Scientific, USA), respectively. After 24 h, the transfection effect was verified by RT-PCR and Western blot. The overexpression vector is provided by the Shanghai Genechem Co.,Ltd . It was injected into the mice through a tail vein and tested 20 days later.

10. Reduced representation bisulfite sequencing (RRBS)

DNA samples were tested. After qualified sample detection, a certain proportion of negative control (lambda DNA) was added. First, DNA samples were digested by methylation-insensitive restriction enzyme MspI. The DNA after the enzyme digestion

The end of the fragment was repaired, A tail was added, and all cytosine was methylated. DNA fragments with a length of 40-220bp were selected for glue cutting (Meissner,2008). Bisulfite was followed after processing (EZ DNA Methylation Gold Kit, Zymo Research), the unmethylated C changed to U (changed to T after PCR amplification), while the methylated C remained unchanged, and then PCR amplification was performed to obtain the final DNA library. After the completion of library construction, Qubit2.0 was used for preliminary quantitation, the library was diluted to 1ng/μl, and then Agilent 2100 was used to detect the length of inserted fragments in the library. After meeting the expectation, q-pcr method was used to accurately quantify the effective concentration of the library (effective concentration of the library >2nM) to ensure library quality. After qualified database inspection, Illumina HiSeq/MiSeq sequencing was performed after pooling of different libraries according to the effective concentration and target depooling data volume requirements.

11.Lipidomics analysis

In this study, liquid mass spectrometry (LC-MS) [29, 30] technology was used to conduct lipidomics research. There were 5 samples in each group. The experimental process mainly included sample collection, lipid extraction, LC-MS/MS detection and data analysis, etc.

12.Echocardiography

At a specified point in time, first using hair removal creams to remove chest hair, in mice and by intraperitoneal injection of 80 mg/ml of sodium pentobarbital anesthesia in mice, by tape will be fixed on the fixed in mice, and the sensor probe was carefully placed on the left side chest between the fourth and sixth frame Then capture m type in papillary muscle level image. Each image loop included 10 to 20cardiac cycles. Data were averaged from at least three cycles per loop. The interventricular septum (IVS), interventricular septal thickness at systolic (IVSs), interventricular septal thickness at diastole

(IVSd), left ventricular posterior wall s (LVPW), left ventricular posterior wall of systolic (LVPWs), left ventricular posterior wall of diastolic (LVPWd) were directly

measured, while other parameters, such as left ventricular end-diastolic volume (LVEDV), left ventricular end-systolic volume (LVESV), ejection fraction (EF), stroke Volume (SV), heart rate (HR), were derived automatically by the Vevo 2,100 imaging system (Visual Sonics,Toronto, ON, Canada).

13. Statistical analysis

The data were analyzed and graphed using GraphPad Prism version 8.0, and all summary data are presented as the mean ± SEM from 2 to 3 independent experiments. The data were analyzed and graphed using GraphPad Prism version 8.0, and all summary data are presented as the mean±SEM from 2 to 3 independent experiments. The sample size required for each experiment is based on the previous research and experimental data. The mice were randomly assigned to different treatment groups. To avoid observation bias, the operator was blindfolded during the selection of mice and samples for echocardiography, histology, simplified methylation sequencing, and lipidomics analysis. The Shapiro-Wilk normality test was used for data distribution normality. The data were normally distributed using unpaired, 2-tailed Student t test (for comparing 2 groups) or 1-way ANOVA with Bonferroni post hoc test (for multi-group comparisons). For data that did not conform to normal distribution, 2-tailed Mann-Whitney U test (for comparing two groups) or Kruskal-Wallis test (for multi-group comparisons) was used. There are no cross-test corrections for multiple tests, only in-test corrections. Representative images were selected according to the values closest to the mean of each group. There is a P value in the Fig, and a value <0.05 is considered statistically significant.

Results

1. PM induced epigenetic alteration and DNA methylation profiling identified the key gene-PDGFRβ in heart tissue of C57BL/6J mice.

In order to explore the epigenetic changes that occur in mouse hearts after a real-ambient PM exposure via an individual ventilated cage (IVC)-based system, we performed reduced representation bisulfite sequencing (RRBS). As can be seen from the distribution map of the number of methylation levels in functional regions, the genes with hypermethylation or hypomethylation were mainly concentrated in intron regions, while the difference between high and low methylation was the largest in repeat region (Fig. 1a). According to the length distribution map of differential methylation region (DMR), the length of DMR is between 0 and 400bp (Fig. 1b). Although the difference in discrete values between the exposed group and the control group was not significant, the distribution of DMRS methylation level in the exposed group was relatively concentrated (Fig. 1c). The heat map analysis of the methylation level in the functional region between the samples showed that there was significant difference methylation between the exposed group and the control group. Among them, there were 3808 (57.66%) hypermethylated genes and 2796 (42.34%) hypomethylated genes (Fig. 1d). GO and KEGG analysis revealed the GO terms and important KEGG pathways which PM may trigger. According to GO analysis

results, in the three aspects of biological process, cell component and molecular function, differentially methylated genes mainly concentrated in the growth and development process of biological process, the development process of anatomical structure, single-multicellular biological process and other categories. In KEGG result analysis, differentially methylated genes mainly regulated the PI3K-Akt signaling pathway, RAS signaling pathway, MAPK signaling pathway and Rap1 signaling pathway. (Fig. 1e and Fig. 1f). Interestingly, the differential methylated gene PDGFRβ in this study was enriched in the MAPK pathway and was associated with multiple pathways. We found that it is closely associated with the downstream MEK/ERK pathway. Overall, we found that PM induced epigenetic changes and RRBS revealed a hypermethylated gene PDGFRβ. Given the established roles of PDGFRβ signaling, we investigated the effects of PDGFRβ and its downstream related pathways in our subsequent experiments.

2. PM induces PDGFRβ hypermethylation mediated MEK/ERK pathway to trigger myocardial hypertrophy in heart tissue of C57BL/6J mice.

Exposing mice to 6 weeks of real-ambient PM via the IVC-based system resulted in a significantly thickened right ventricular wall in mice (Fig. 2a, b, c). To verify the methylation status of PDGFRβ, in the following RT-qPCR analysis, compared with the control group, the mRNA expression level of PDGFRβ in the PM exposure group showed a significantly decreased trend, which was also consistent with the results of the RRBS analysis (Fig. 2d). Western blot analysis also showed that the protein levels of RAS, RAF, MEK and ERK, which are downstream of PDGFRβ via the MEK/ERK pathway, showed a downward turn in the PM exposure group compared to control (Fig. 2e, f, g, l). Hence, our results indicate that PM directly leads to cardiac hypertrophy and hypermethylation of PDGFRβ in mice, which leads to down-regulation of the expression levels of related genes in its downstream MEK/ERK pathway.

MEK/ERK pathway is closely related to cardiac hypertrophy. In order to further understand the mechanism of MEK/ERK pathway induced cardiac hypertrophy after PDGFRβ hypermethylation, primary neonatal rat cardiomyocytes were exposed to different concentrations of PM. CCK8 assay showed a stress-induced increase in cell viability at 25 μg/mL, and then showed a dose-dependent decrease with the increase of PM concentration (Fig. 3a). Finally, we selected three different PM concentrations for further study. The results of RT-qPCR showed that the mRNA expression levels of PDGFRβ and downstream RAS, RAF, MEK and ERK all decreased with increased PM concentrations (Fig. 3b, c, d, e, f). Importantly, these results were consistent with western blot analysis of protein expression (Fig. 3g, h, j, k, l). Based upon these data, we chose 50μg/ mL PM as our experimental concentration for future experiments. However, we also know that PM exposure time has a significant effect on experimental results. To assess this, we established PM exposure models at different time points in primary neonatal rat cardiomyocytes to detect the expression of myocardial hypertrophy markers. RT-qPCR results showed that mRNA levels of cardiac hypertrophy related markers in cardiomyocytes showed an upward trend during the first 0-6 hours of PM exposure. This was followed by a decrease in mRNA expression during the 6-24 hours timepoints (Fig. 3m, n, o). Based upon these results, we conducted the study after 6 hours of PM exposure. We found that when PM concentration was 50μg/ mL and exposure time was 6 hours,

the mRNA expression levels of the three DNA methyltransferases followed an upward trend (Fig. 3p, q, r). Thence, we conclude that exposing cardiomyocytes to PM at 50 μg/mL for 6 hours causes changes in DNA methylation levels in cardiomyocytes and may affect cardiac hypertrophy.

3. Effects of up-regulation of PDGFRβ on MEK/ERK pathway and cardiac hypertrophy in cardiomyocytes.

To investigate the effect of PDGFRβ on MEK/ERK pathway and cardiac hypertrophy. We used a recombinant enhanced green fluorescent protein (EGFP) plasmid with high expression of PDGFRβ (hPDGFRβ) and an empty plasmid (PDGFRβ-con) for transient gene transfection in cardiomyocytes after PM exposure. Fluorescence images demonstrate that the transfection was successful (Fig. 4a). Then we performed RT-qPCR and WB to verify that overexpression was achieved. The mRNA level of hPDGFRβ was 28 times higher than that of blank control and PDGFRβ-con (Fig. 4b). The expression level of the protein was also consistent with that of RT-qPCR (Fig. 4c). We found that RT-qPCR results showed that mRNA expression levels of RAS, RAF, MEK and ERK were significantly decreased in the PM exposure group compared with the control group, which was consistent with the results of real PM exposure in our previous animal experiments. The mRNA expression levels of RAS, RAF, MEK and ERK in the hPDGFRβ group showed an upward trend (Fig. 4d, e, f, g), and the protein expression levels of MEK and ERK in the WB experiment were also consistent with the results of RT-qPCR (Fig. 4h, I, j). We further verified the effect of hPDGFRβ on cardiac hypertrophy markers by RT-qPCR. We found that the mRNA expression levels of atrial natriuretic factors (ANF), brain natriuretic factor (BNF) and beta-myosin heavy chain (β-MHC) were significantly increased in the PM exposure group, which was consistent with the results of our previous experiment. The mRNA expression levels of ANF, BNF and β-MHC in hPDGFRβ group showed a decreasing trend (Fig. 4k, l, m). These results suggest that high expression of PDGFRβ facilitates increased activation of the MEK/ERK pathway, thereby preventing the increase in cardiac hypertrophy markers, suggesting a net effect ofreducing cardiac hypertrophy.

4. Effect of inhibiting methylation on MEK/ERK pathway and cardiac hypertrophy in cardiomyocytes.

In order to further explore the effects of PDGFRβ methylation on MEK, ERK pathways and cardiac hypertrophy, we established a methylation inhibition model in primary neonatal rat cardiomyocytes. Firstly, CCK8 experiments were conducted to understand the effects of different concentrations of methylation inhibitors (5-Azacytidine: 5AZA) on cell viability (Fig. 5a). According to RT-qPCR results, when the concentration of 5AZA was 10μM, the mRNA expression level of DNA methyltransferase 1(DNMT1) and DNA methyltransferase 3A (DNMT3A) could be decreased (Fig 5b, c), so we chose 10μM as our experimental concentration. We found that the mRNA expression levels of MEK, ERK, RAS and RAF in the methylation inhibitor group showed an upward trend compared with the PM exposure group (Fig. 5d, e, f, g). In the western blot results, the protein expression levels of MEK and ERK were also consistent with the RT-qPCR results (Fig. 5h, I, j). In order to further study the effect of methylation inhibitors on cardiac hypertrophy, we used RT-qPCR to observe the expression levels of markers related to cardiac hypertrophy. We found that compared with PM exposure group, the mRNA expression levels of ANF, BNF and β-MHC in the methylation inhibitor group showed a decreasing trend (Fig. 5k, l, m). These results indicated that the

methylation inhibitor group activated the MEK/ERK pathway, reduced the effect of cardiac hypertrophy, and had a protective effect on cardiomyocytes.

5. Effects of up-regulation of PDGFRβ on MEK/ERK pathway and cardiac hypertrophy in heart tissue of C57BL/6J mice.

Since the activation of cardiac-specific transgenic PDGFRβ has a significant effect, we further investigated the regulatory mechanism of high expression of PDGFRβ on cardiotoxicity induced by PM exposure in mice and the potential of PDGFRβ in improving cardiac hypertrophy outcomes. Our adenovirus helper-free system is composed of three plasmids, namely a viral vector, PAAV-RC vector and pHelper vector. We generated AAV9: Ubi by using myocardial cell-specific ubiquitination protein promoter and triple FIAG marker.3Flag-PDGFR β (hPDGFRβ), as a control, we generated AAV9: Ubi-EGFP (hPDGFRβ-Con), and replaced 3Flag-PDGFR β with EGFP (Fig. 6a). AAV9 was first injected into mice by tail vein, and PDGFRβ expression was highly specific in the heart after 20 days. The high expression of PDGFRβ was clearly observed under the light microscope by immunohistochemical experiments, and the green fluorescence of AAV9 in the heart tissue was directly observed by frozen sections, which was consistent with the immunohistochemical results (Fig. 6c). In addition, we also examined the expression level of PDGFRβ protein by western blot assay, and we found that the protein expression level of PDGFRβ group was higher than that of hPDGFRβ-con group (Fig. 6d), so 20 days later, the PDGFRβ high expression model was established. Then we performed tracheal drip, once a week, where the PM of tracheal drip came from IVC-based real-ambient PM exposure system, and the total concentration of tracheal drip was consistent with the total concentration in real-ambient PM exposure system (Fig. 6b). Then we conducted echocardiographic examination of the mice, and it was found that interventricular septum (IVS), interventricular septal thickness at systolic (IVSs), interventricular septal thickness at diastole (IVSd), left ventricular posterior wall (LVPW), left ventricular posterior wall of systolic (LVPWs), left ventricular posterior wall of diastolic (LVPWd) in the PM exposed group showed an increasing trend compared with the control group, indicating that myocardial hypertrophy appeared in the exposed group. Compared with PM exposure group, hPDGFRβ group showed a decreasing trend in all indicators (Fig. 6e, f, g, h, i, j), indicating that hPDGFRβ can reduce cardiac hypertrophy and thus protect the heart. To follow up these data, we further studied this mechanism. We used western blot experiments to study the related genes in the downstream pathway of PDGFRβ. We observed that RAS, RAF, MEK, pMEK, ERK and pERK in the downstream pathway all showed the negative same trend. The protein expression level showed an upward trend (Fig. 6k, l, m, o, p, q), which was consistent with the results of our previous cell experiments. In conclusion, hPDGFRβ activates downstream MEK and ERK pathways, ameliorates the effects of cardiac hypertrophy and protects the mouse heart.

6. PM - induced myocardial hypertrophy and lipid metabolism disorders.

These data have demonstrated that PM exposure can lead to cardiac hypertrophy in mice. However, whilst is well known that cardiac hypertrophy is closely related to lipid metabolism, we next asked how is PDGFRβ related to lipid metabolism? To further explore the relationship between the two, we first used HE

staining to observe the relationship between the PM exposure group and the control group in AC16 cells (Fig. 7a). We found that compared with the control group, the cardiomyocytes in the exposed group showed a decreased nucleo-plasmic ratio (Fig. 7b) and an increased area ratio (Fig. 7c), combined with our previous experimental results in primary neonatal rat cardiomyocytes, indicating that PM exposure did cause myocardial hypertrophy in cardiomyocytes. Next, oil red O staining was used to stain AC16, and we observed that the PM exposure group had significant lipid accumulation (Fig. 7d). Subsequently, oil red O staining was used to observe the heart tissues of the tracheal drip group and the control group, and it was found that the tracheal drip group also had a small amount of lipid accumulation (Fig. 7e).

In summary, PM exposure can lead to lipid metabolism disorder in the mouse heart. Since PPARα and PPARγ are closely related to lipid metabolism, we first used western blot analysis to investigate changes in PPARα and PPARγ protein expression in the heart tissue of real-ambient PM exposure system. We found that the protein expression levels of PPARα and PPARγ in the PM exposure group were increased compared with the control group (Fig. 7f, g, h). Further, PM exposure is closely related to cardiac lipid metabolism. And how does this relate to PDGFRβ? As a result, we established a model of PDGFRβ overexpression in AC16 cells. Using western blot experiments, we found that PPARα protein expression was increased in the PM-exposed group compared with the control group, consistent with previous results, but PPARα protein expression was lower in the hPDGFRβ group than in the exposed group (Fig. 7i, j). Similarly, we also obtained consistent results in the high expression model of PDGFRβ after tracheal drip, with PPARα protein expression increased in the PM exposure group compared with the control group, but decreased in the hPDGFRβ group compared with the exposure group (Fig. 7k, l). In conclusion, hPDGFRβ protects the mouse heart by alleviating PM-induced lipid metabolism disturbances in cardiomyocytes and the mouse heart.

In order to further study the PM induced changes in lipid metabolism, we performed lipidomics analysis using LC-MS high-throughput analysis technology in the tracheal drip mode. Firstly, in the lipid subclass analysis, a total of 14 lipid molecules were detected in the positive ion mode, which were phosphatidylcholine(PC), phosphatidylethanolamine (PE), phosphatidylserine (PS), phosphatidylglycerol (PG), phosphatidic acid (PA), Cardiolipin (CL), sphingomyelin (SM), ceramide (Cer), glucosylceramides (GlcCer), diacylglycerols (DAG), triacylglycerols (TAG), a to carotenoids (ACar), bone morphogenetic protein (BMP) and human bone morphogenetic protein (HBMP). Among them, PC has the most subcategories, up to 348, and TAG has 219 subcategories (Fig. 8a). A total of 16 lipid molecules were detected in negative ion mode, which were PC, PE, PS, phosphatidylinositol (PI), PG, PA, CL, SM, Cer, GlcCer, monogalactosyldiacylglycerol (MGDG), sulfoquinovosyldiacylglycerol (SQDG), fatty acid esters of hydroxy fatty acids (FAHFA), HBMP and ganglioside (GM3). Among them, PC has the most subtypes, with 101 species, followed by PE with 90 species (Fig. 8b). We found that the PC subclass was highest in both positive and negative ion modes. Further analysis of the different lipid compounds revealed that a total of 1226 differential lipid compounds were detected in positive ion mode, among which 34 which were significantly different, 30 which were significantly up-regulated and 4 which were significantly down-regulated. In the negative ion mode, a total of 582 different lipid compounds were detected, among which 38 were significantly different, 29 were significantly up-regulated and 9 were significantly down-regulated.

Then, we observed the overall distribution of different lipid compounds from the volcano diagram. It could be seen intuitively that no matter in the positive ion mode or the negative ion mode, more lipid compounds were up-regulated than down-regulated, and the expression multiple of lipid compounds in different groups changed significantly (Fig. 8c, d). So, we then looked at the fold change (FC) analysis of differential lipid compounds and found that in the positive ion mode, Creatine had the largest differential multiple, followed by canrenone. In the negative ion mode, carnosine had the largest differential multiple, followed by L-Histidine (Fig. 8e, f). In order to compare the differences of metabolic expression patterns between two groups and within the same comparison group, hierarchical cluster analysis was performed on the obtained metabolites. We found significant differences between the control group and the exposed group (Fig. 8g, h). In order to check the consistency of lipid compounds and lipid compounds, Pearson correlation coefficient between all lipid compounds was calculated to analyze the correlation between each lipid compound. We found that as the linear relationship between the two lipid compounds increased, the positive correlation tended to 1, and the negative correlation tended to -1(Fig. 8i, j). In general, these data suggest that PM exposure can lead to changes in cardiac lipid metabolism in mice.

Discussion

One of the most important findings of this study is that we demonstrate for the first time that PM-induced PDGFRβ methylation induces cardiac hypertrophy and that this PM-induced PDGFRβ methylation is also closely associated with myocardial lipid toxicity. Interestingly, high expression of PDGFRβ mitigated this hypertrophy and myocardial lipid toxicity. This activity was demonstrated in PDGFRβ -overexpressed mouse heart and neonatal mouse primary cardiomyocytes, as well as in human cardiomyocytes AC16.The effects of PDGFRβ methylation on myocardial hypertrophy and myocardial lipid toxicity define the important role of PDGFRβ in maintaining cardiac stability.

Gene methylation is a common form of modification in eukaryotic cells and a major epigenetic form of gene expression regulation in mammals, which may provide a clearer understanding of the molecular mechanism of cardiac hypertrophy by PM [1-3, 7, 10, 31]. Myocardial hypertrophy affects the structure and function of the heart in a variety of ways, resulting in myocardial lipotoxicity [17, 32]. However, the relationship between PM-induced hypertrophy and myocardial lipotoxicity has not been reported. Given its unique role in these processes, PM-induced gene methylation is an important target for studying myocardial hypertrophy and myocardial lipotoxicity.

The PM component is very complex. PM exposure not only increases the risk of cardiovascular disease, particles with small particle size (such as $PM_{2.5}$ and $PM_{0.1}$) can directly enter alveolar deposition and enter the body through blood circulation, causing serious damage to human organs. Studies have shown that a thickening of the right ventricular wall, which is typical after lung injury [33]. Since the right ventricle is usually associated with cardiopulmonary effects, the changes we observed suggest that PM exposure may be related to the pulmonary system and the right ventricle. It's worth noting that, our previous study has analyzed the composition and exposure concentration of PM [11], but it is not yet possible to detect all components of PM in blood. In addition, we also performed ICP mass spectrometry

analysis of metal content in mouse hearts, and found deposition of Na, K, Se and Fe in PM exposure group [12]. Deposition of some metals is known to alter DNA methylation patterns in genes, leading to the development of a range of diseases [34,35].

Therefore, RRBS was performed on C57BL/6J mice in the individual ventilated cage (IVC)-based real-ambient PM exposure system. In our model of real-ambient PM exposure system, reduced representation bisulfite sequencing (RRBS) identified one of the key genes, PDGFRβ, that is involved in the regulation of multiple pathways, especially the MEK/ERK pathway in the MAPK pathway. Activation of PDGFRβ, a platelet-derived growth factor receptor, regulates myocardial infarction healing and angiogenesis. PDGFRβ is also associated with myocardial cell proliferation and myocardial regeneration [36,37]. The MEK/ERK pathway is one of the most studied signaling pathways because it controls many important cellular mechanisms [38]. The MEK/ERK pathway may occupy a central regulatory position in the signaling layer of cardiomyocytes because of its unique ability to respond to almost all of the characteristic hypertrophy agonists and stress stimuli examined to date, based on its ability to promote cardiomyocyte growth in vitro [39]. However, the role of MEK/ERK in regulating cardiac hypertrophy is currently an area of ongoing debate [38]. Studies have shown that ERKs is one of the necessary conditions for inducing cardiac hypertrophy [40,41]. Other studies have shown that activation of ERKs is associated with the prevention of cardiomyocyte hypertrophy [42]. In the real-ambient PM exposure system, we found that the mRNA and protein expression levels of MEK and ERK in the downstream PDGFRβ pathway decreased in the PM exposure group, suggesting that PM-induced PDGFRβ methylation leads to the down-regulation of PDGFRβ expression and inhibits the expression of genes related to the downstream pathway, leading to myocardial hypertrophy.

Most studies on PM toxicity have been validated in the cardiovascular system and endothelial cells. However, studies on PM-induced cardiomyocyte related toxicity are limited [43]. It is well known that different concentrations of PM have a bipolar effect on cell growth. Low concentrations of PM can promote cell proliferation, while high concentrations can inhibit cell proliferation [44,45]. Although numerous studies have shown that the cytotoxicity of PM depends on its concentration [46], the effects of PM exposure time on cells are different [47,48]. Some studies have shown that long-term exposure increases the risk of cardiovascular death more than short-term exposure [49]. Other studies have found that short-term PM exposure leads to intense vascular remodeling and exacerbates the transition from left ventricular failure to right ventricular hypertrophy [50,51]. So, in order to meet the relevant requirements of myocardial hypertrophy and methylation, we finally selected concentration of PM exposure was 50 μg/mL and PM exposure time of 6 hours in primary neonatal rat cardiomyocytes. We know that DNA methyltransferase catalyzes DNA methylation [52,53]. At the same time, the above experimental conditions also satisfied the expression of three DNA methyltransferases.

Our study is the first to show that real-ambient PM exposure leads to changes in PDGFRβ methylation levels. The role of PDGFRβ signaling in angiogenesis and early hematopoiesis has also been established. PDGFRβ is involved in a variety of well-defined signaling pathways, such as MRK/ERK-MAPK, PI3K, and PLC-γ, and is involved in a variety of cellular and developmental responses [26]. However, the mechanism

described here of PDGFRβ methylation induced cardiotoxicity by PM exposure is novel. To further investigate this, we overexpressed PDGFRβ in primary cardiomyocytes and utilized methylation inhibition. We found that the expression of MEK, ERK was significantly increased in the hPDGFRβ group, and the expression of myocardial hypertrophic markers was significantly decreased in the hPDGFRβ group, suggesting that MEK/ERK pathway was activated in the hPDGFRβ group and the effect of myocardial hypertrophy was inhibited. At this point, it is not clear that PDGFRβ methylation affects the downstream pathway, so the methylation inhibitor 5-Azacytidine(5AZA) was used to inhibit the methylation of cells. 5-Azacytidine is a kind of deoxycytidine analogue, usually used for demethylation through promoters [54,55]. We found that the methylation inhibitor group also significantly increased the expression levels of MEK and ERK, while significantly reduced the expression levels of markers of cardiac hypertrophy. These results indicated that methylation inhibitor group activated MEK/ERK pathway and inhibited myocardial hypertrophy effect, which was consistent with PDGFRβ high expression group. In summary, PM exposure leads to methylation of PDGFRβ in primary cardiomyocytes, resulting in decreased gene expression in the downstream MEK/ERK pathway and ultimately cardiac hypertrophy. However, high expression of PDGFRβ and methylation inhibition improved myocardial hypertrophy, thereby protecting myocardial cells. This is also the first time that we found the protective effect of high expression of PDGFRβ on the heart under PM exposure.

Adeno-associated virus (AAV) is known to be an unenveloped virus that can be engineered to deliver DNA to target cells. Recombinant AAV particles of DNA sequences for a variety of therapeutic applications have proven to be one of the safest strategies for gene therapy to date [56]. In laboratory studies, PM of tracheal drip are often seen to negatively affect cardiovascular activities such as heart function, blood pressure and cardiomyopathy [57]. Similarly, in the mouse heart, the continuous activation of PDGFR-β signal mediated by AAV9 vector can also improve myocardial hypertrophy caused by tracheal drip, providing gene therapy strategies for reducing myocardial hypertrophy.

Related studies have shown that cardiac hypertrophy is closely related to myocardial metabolism, and lipid overload can cause cardiac hypertrophy and cardiac dysfunction [58-60]. PM has been found to cause cardiac hypertrophy [31], however, no studies related to cardiac lipid metabolism caused by PM have been reported so far. Upfront we found PM group exposed mice displayed right ventricular free wall thickening [10,11]. In cardiomyocytes, we found a decreased nucleo-plasmic ratio in PM exposed cardiomyocytes [61], area ratio increases [62,63]. All three markers of cardiac hypertrophy were elevated in the PM exposure group and significantly decreased in the PDGFRβ group. Importantly, we also found lipid deposition in both the mouse heart and myocardial cells in the PM exposed group. It is well known that lipid deposition is closely related to lipid metabolism [64-66]. Lipids participate in regulating various biological activities, including energy conversion, material transport, information identification and transmission, cell growth and differentiation, and apoptosis, and abnormal lipid metabolism is closely associated with a variety of disease occurrence, development, such as atherosclerosis, diabetes, obesity, alzheimer's disease and cancer, etc [67-70]. So we asked, is PM exposure associated with myocardial hypertrophy associated with myocardial lipid metabolism disorders? Can this myocardial lipid metabolism disorder be improved by high PDGFRβ expression? PPARα and PPARγ can play an important

role in metabolic regulation at the transcriptional level, and play a very important role in lipid metabolism. The increase or decrease of PPARα and PPARγ expression levels may lead to lipid metabolism disorder [71-75]. However, under normal physiological conditions, the expression in cardiomyocytes is low and participates in lipid metabolism balance [76]. In our study, we found that the expression levels of PPARα and PPARγ increased in PM exposure group, and the protein expression of PPARα decreased in PDGFRβ high expression group, which was not consistent with normal physiological conditions.

The lipids DAG, Cer and PA and so on, are basic components of membrane and intermediate of lipid metabolism, are key elements of lipid signal transduction and play an important role in lipid toxicity [77-79]. However, interestingly, lipidomic [80-82]. analysis showed that these major lipid compounds, such as DAG, Cer and PA, which make up the membrane components, were significantly different lipid compounds in the control and PM exposed groups. So we linked lipid toxicity to PDGFRβ, a receptor on the cell membrane. Our studies have shown that PM exposure leads to hypermethylation of PDGFRβ and ultimately to myocardial hypertrophy. Now, we have concluded that PM exposure causes myocardial lipotoxicity. The myocardial lipotoxicity was associated with PDGFRβ. In addition, hPDGFRβ was found to ameliorate this PM induced myocardial lipid toxicity in our study.

In summary, PM exposure can lead to methylation of PDGFRβ gene and inhibit the effect of downstream MEK/ERK pathway on myocardial hypertrophy. Simultaneous activation of PPARα and PPARγ leads to myocardial lipotoxicity. So, the activation of PDGFR-β signaling is a potential strategy to promote cardiac function by improving myocardial hypertrophy and myocardial lipotoxicity.

Abbreviations

PDGFRβ	a platelet-derived growth factor receptor β
PM	particulate matter
CVD	cardiovascular disease
PPARα	peroxisomal proliferator-activated receptor -α
PPARγ	peroxisomal proliferator-activated receptor -γ
RRBS	reduced representation bisulfite sequencing
LC-MS	lipidomics mass
IVC	individual ventilated cage
DMR	differential methylation region
ANF	atrial natriuretic factors
BNF	brain natriuretic factor
β-MHC	β-myosin heavy chain
5AZA	5-Azacytidine
DNMT1	DNA methyltransferase 1
DNMT3A	DNA methyltransferase3A
DNMT3B	DNA methyltransferase 3B
IVS	interventricular septum
IVSs	interventricular septal thickness at systolic
IVSd	interventricular septal thickness at diastole
LVPW	left ventricular posterior wall
LVPWs	left ventricular posterior wall of systolic
LVPWd	left ventricular posterior wall of diastolic
PC	phosphatidylcholine
PE	phosphatidylethanolamine
PS	phosphatidylserine
PG	phosphatidylglycerol
PA	phosphatidic acid
CL	cardiolipin
SM	sphingomyelin

Cer	ceramide
GlcCer	glucosylceramides
DAG	diacylglycerols
TAG	triacylglycerols
ACar	a to carotenoids
BMP	bone morphogenetic protein
HBMP	human bone morphogenetic protein
PI	phosphatidylinositol
MGDG	monogalactosyldiacylglycerol
SQDG	sulfoquinovosyldiacylglycerol
FAHFA	fatty acid esters of hydroxy fatty acids
GM3	ganglioside
EGFP	enhanced green fluorescent protein

Declarations

Acknowledgments

Corresponding authors: Lianhua Cui, Qingdao University, School of Public Health, 16 Ningde Road, Qingdao, Shandong, 266021, China. Or Yuxin Zheng, Qingdao University, School of Public Health, 16 Ningde Road, Qingdao, Shandong, 266021, China.

We are grateful to Xinyu Dun for conducting the experiment of tracheal dripping in animal experiments, we thank Benying Li tail intravenous injection experiment was carried out and the data collection, with the help of Hongxu Bao for all animal breeding and the extraction of particulate matter, Zijian Xu analyzed the data and preparing the corresponding graphics, with the help of Andong Ji, primary myocardial cells were extracted for cell experiments. We are grateful to Hebei Medical University for providing the real-ambient PM exposure system. With the help of Rong Zhang, our real-ambient PM exposure system went smoothly. Daochuan Li provided technical methods and guidance for animal experiments and provided important feedback. Ying Zhang completed all the molecular experiments. Ying Zhang and Xinyu Dun drafted the paper and designed the charts. Thanks to medical Science of Qingdao University for providing the pilot experiment. Rui Chen provided important feedback for this article. We thank Zhezhen Jin for providing statistical analysis and text proofreading, Jianxun Wang for providing primary myocardial cells culture technical guidance, Lianhua Cui designed the study and revised the manuscript, provided funding and important feedback for this article. Lianhua Cui and Yuxin Zheng analyzed the paper and

conceptualized, funded and supervised the final draft. All authors provided feedback on the research, analysis and articles.

Sources of Funding

This study was supported by research grants from the National Natural Science Foundation of China (81872591), Key project of major Research Program of National Natural Science Foundation of China (91943301), Natural Science Foundation of Shandong Province, China (ZR2019MH028).

Compliance with ethical standards

Conflict of interest.

The authors declare that they have no conflict of interest.

References

1. Marchini T, Zirlik A, Wolf D. Role of Air Pollution Particulate Matter in Cardiometabolic Disease: Evidence from Mice and Humans. Pathogenic. 2020;33:263–279.
2. Tian M, Zhao J, Mi X, Wang K, Kong D, Mao H, Wang T. Progress in research on effect of PM2.5 on occurrence and development of atherosclerosis. J Appl Toxicol. 2021;41:668–682.
3. Liang F, Liu F, Huang K, Yang X, Li J, Xiao Q, Chen J, Liu X, Cao J, Shen C, et al. Long-Term Exposure to Fine Particulate Matter and Cardiovascular Disease in China. American College of Cardiology. 2020;75:707–717.
4. Weichenthal S, Lavigne E, Evans G, Pollitt K, Burnett RT. Ambient PM2.5 and risk of emergency room visits for myocardial infarction: impact of regional PM2.5 oxidative potential: a case-crossover study. Environ Health. 2016;15:46.
5. Shah AS, Lee KK, Mcallister DA, Hunter A, Nair H, Whiteley W, Langrish JP, Newby DE, Mills NL. Short term exposure to air pollution and stroke: systematic review and meta-analysis. BMJ. 2015;350: h1295.
6. Wang M, Zhou T, Song Y, Li X, Ma H, Hu Y, Heianza Y, Qi L. Joint exposure to various ambient air pollutants and incident heart failure: a prospective analysis in UK Biobank. Eur Heart J. 2021;42:1582–1591.
7. Martinelli N, Olivieri O, Girelli D. Air particulate matter and cardiovascular disease: a narrative review. Eur J Intern Med. 2013;24:295–302.
8. Marris CR, Kompella SN, Miller MR, Incardona JP, Brette F, Hancox JC, Sørhus E, Shiels HA. Polyaromatic hydrocarbons in pollution: a heart-breaking matter. J Physiol. 2020;598:227–247.
9. Su X, Tian J, Li B, Zhou L, Kang H, Pei Z, Zhang M, Li C, Wu M, Wang Q, et al. Ambient PM2.5 caused cardiac dysfunction through FoxO1-targeted cardiac hypertrophy and macrophage-activated fibrosis in mice. Chemosphere. 2020;247: 125881.

10. Cui L, Shi L, Li D, Li X, Su X, Chen L, Jiang Q, Jiang M, Luo J, Ji A, et al. Real-Ambient Particulate Matter Exposure-Induced Cardiotoxicity in C57/B6 Mice. Frontiers in pharmacology. 2020;11:199.
11. Jiang Q, Ji A, Li D, Shi L, Gao M, Lv N, Zhang Y, Zhang R, Chen R, Chen W, et al. Mitochondria damage in ambient particulate matter induced cardiotoxicity: Roles of PPAR alpha/PGC-1 alpha signaling. Environ Pollut. 2021;288:117792.
12. Cui L, Shi L, Li D, Li X, Su X, Chen L, Jiang Q, Jiang M, Luo J, Ji A, et al. Real-Ambient Particulate Matter Exposure-Induced Cardiotoxicity in C57/B6 Mice. Front Pharmacol. 2020;11:199.
13. Sun B, Shi Y, Yang X, Zhao T, Duan J, Sun Z. DNA methylation: A critical epigenetic mechanism underlying the detrimental effects of airborne particulate matter. Ecotoxicol Environ Saf. 2018;161:173–183.
14. Lei H, Hu J, Sun K, Xu D. The role and molecular mechanism of epigenetics in cardiac hypertrophy. Heart failure reviews. 2020.
15. Micheu MM, Birsan MV, Szép R, Keresztesi Á, and Nita IA. From air pollution to cardiovascular diseases: the emerging role of epigenetics. Molecular biology reports. 2020;47:5559–5567.
16. Nakamura M, Sadoshima J. Mechanisms of physiological and pathological cardiac hypertrophy. Nat Rev Cardiol. 2018;15:387–407.
17. Kolwicz SC, Jr., Purohit S,Tian R. Cardiac metabolism and its interactions with contraction, growth, and survival of cardiomyocytes. Circ Res. 2013;113:603–16.
18. Di Paolo G, De Camilli P. Phosphoinositides in cell regulation and membrane dynamics. Nature. 2006;443:651–7.
19. Cartier A, Hla T. Sphingosine 1-phosphate: Lipid signaling in pathology and therapy. Science. 2019;366.
20. Al-Sulaiti H, Diboun I, Banu S, Al-Emadi M, Amani P, Harvey TM, Domling AS, Latiff A, Elrayess MA. Triglyceride profiling in adipose tissues from obese insulin sensitive, insulin resistant and type 2 diabetes mellitus individuals. J Transl Med. 2018;16: 175.
21. Margolis M, Perez O, Jr., Martinez M, Santander AM, Mendez AJ, Nadji M, Nayer A, Bhattacharya S, Torroella-Kouri M. Phospholipid makeup of the breast adipose tissue is impacted by obesity and mammary cancer in the mouse: Results of a pilot study. Biochimie. 2015;108:133–9.
22. Warren JS, Oka SI, Zablocki D, Sadoshima J. Metabolic reprogramming via PPARalpha signaling in cardiac hypertrophy and failure: From metabolomics to epigenetics. Am J Physiol Heart Circ Physiol. 2017;313:H584-H596.
23. Krishnan J, Suter M, Windak R, Krebs T, Felley A, Montessuit C, Tokarska-Schlattner M, Aasum E, Bogdanova A, Perriard E, et al. Activation of a HIF1alpha-PPARgamma axis underlies the integration of glycolytic and lipid anabolic pathways in pathologic cardiac hypertrophy. Cell Metab. 2009;9:512–24.
24. Hoch RV, Soriano P. Roles of PDGF in animal development. Development. 2003;130: 4769–84.

25. Bjarnegård M, Enge M, Norlin J, Gustafsdottir S, Fredriksson S, Abramsson A, Takemoto M, Gustafsson E, Fässler R, Betsholtz C. Endothelium-specific ablation of PDGFB leads to pericyte loss and glomerular, cardiac and placental abnormalities. Development. 2004;131:1847–57.
26. Andrae J, Gallini R, Betsholtz C. Role of platelet-derived growth factors in physiology and medicine. Genes Dev. 2008;22:1276–312.
27. Li D, Zhang R, Cui L, Chu C, Zhang H, Sun H, Luo J, Zhou L, Chen L, Cui J, et al. Multiple organ injury in male C57BL/6J mice exposed to ambient particulate matter in a real-ambient PM exposure system in Shijiazhuang, China. Environ Pollut. 2019;248:874–887.
28. Jiang Q, Lust RM, Strynar MJ, Dagnino S, Dewitt JC. Perflurooctanoic acid induces developmental cardiotoxicity in chicken embryos and hatchlings. Toxicology 293: 97–106.
29. Want EJ, Wilson ID, Gika H, Theodoridis G, Plumb RS, Shockcor J, Holmes E, Nicholson JK. Global metabolic profiling procedures for urine using UPLC-MS. Nat Protoc. 2010;5: 1005–18.
30. Dunn WB, Broadhurst D, Begley P, Zelena E, Francis-Mcintyre S, Anderson N, Brown M, Knowles JD, Halsall A, Haselden JN, et al. Procedures for large-scale metabolic profiling of serum and plasma using gas chromatography and liquid chromatography coupled to mass spectrometry. Nat Protoc. 2011;6:1060–83.
31. Xing Q, Wu M, Chen R, Liang G, Duan H, Li S, Wang Y, Wang L, An C, Qin G, et al. Comparative studies on regional variations in PM2.5 in the induction of myocardial hypertrophy in mice. Sci Total Environ. 2021;775:145179.
32. Wende AR, Symons JD, Abel ED. Mechanisms of lipotoxicity in the cardiovascular system. Curr Hypertens Rep. 2012;14:517–31.
33. Vonk Noordegraaf A, Westerhof BE, Westerhof N. The Relationship Between the Right Ventricle and its Load in Pulmonary Hypertension. J Am Coll Cardiol. 2017;69:236–243.
34. Brocato J, Costa M. Basic mechanics of DNA methylation and the unique landscape of the DNA methylome in metal-induced carcinogenesis. Crit Rev Toxicol. 2013;43:493–514.
35. Nwanaji-Enwerem JC, Colicino E, Specht AJ, Gao X, Wang C, Vokonas P, Weisskopf MG, Boyer EW, Baccarelli AA, Schwartz J. Individual species and cumulative mixture relationships of 24-hour urine metal concentrations with DNA methylation age variables in older men. Environ Res. 2020;186:109573.
36. Yue Z, Chen J, Lian H, Pei J, Li Y, Chen X, Song S, Xia J, Zhou B, Feng J, et al. PDGFR-beta Signaling Regulates Cardiomyocyte Proliferation and Myocardial Regeneration. Cell Rep. 2019;28:966–978 e4.
37. Zymek P, Bujak M, Chatila K, Cieslak A, Thakker G, Entman ML, Frangogiannis NG. The role of platelet-derived growth factor signaling in healing myocardial infarcts. J Am Coll Cardiol. 2006;48:2315–23.
38. Bueno OF, De Windt LJ, Tymitz KM, Witt SA, Kimball TR, Klevitsky R, Hewett TE, Jones SP, Lefer DJ, Peng CF, et al. The MEK1-ERK1/2 signaling pathway promotes compensated cardiac hypertrophy in transgenic mice. EMBO J. 2000;19:6341–50.

39. Bueno OF, Molkentin JD. Involvement of extracellular signal-regulated kinases 1/2 in cardiac hypertrophy and cell death. Circ Res. 2002;91:776–81.
40. Glennon PE, Kaddoura S, Sale EM, Sale GJ, Fuller SJ, Sugden PH. Depletion of mitogen-activated protein kinase using an antisense oligodeoxynucleotide approach downregulates the phenylephrine-induced hypertrophic response in rat cardiac myocytes. Circ Res. 1996;78:954–61.
41. Clerk A, Michael A, Sugden PH. Stimulation of the p38 mitogen-activated protein kinase pathway in neonatal rat ventricular myocytes by the G protein-coupled receptor agonists, endothelin-1 and phenylephrine: a role in cardiac myocyte hypertrophy? J Cell Biol. 1998;142: 523–35.
42. Silberbach M, Gorenc T, Hershberger RE, Stork PJ, Steyger PS, Roberts CT, Jr. Extracellular signal-regulated protein kinase activation is required for the anti-hypertrophic effect of atrial natriuretic factor in neonatal rat ventricular myocytes. J Biol Chem. 1999;274:24858–64.
43. Feng L, Yang X, Asweto CO, Wu J, Zhang Y, Hu H, Shi Y, Duan J, Sun Z. Genome-wide transcriptional analysis of cardiovascular-related genes and pathways induced by PM2.5 in human myocardial cells. Environ Sci Pollut Res Int. 2017;24:11683–11693.
44. Deng F, Guo X, Liu H, Fang X, Yang M, Chen W. Effects of dust storm PM2.5 on cell proliferation and cell cycle in human lung fibroblasts. Toxicol In Vitro. 2007;21:632–8.
45. Xiao T, Ling M, Xu H, Luo F, Xue J, Chen C, Bai J, Zhang Q, Wang Y, Bian Q, et al. NF-kappaB-regulation of miR-155, via SOCS1/STAT3, is involved in the PM2.5-accelerated cell cycle and proliferation of human bronchial epithelial cells. Toxicol Appl Pharmacol. 2019;377:114616.
46. Pope CA, 3rd, Burnett RT, Thun MJ, Calle EE, Krewski DK, Thurston GD. Lung cancer, cardiopulmonary mortality, and long-term exposure to fine particulate air pollution. JAMA. 2002;287:1132–41.
47. Pekkanen J, Kulmala M. Exposure assessment of ultrafine particles in epidemiologic time-series studies. Scand J Work Environ Health 30 Suppl. 2004;2:9–18.
48. Happo MS, Salonen RO, Halinen AI, Jalava PI, Pennanen AS, Kosma VM, Sillanpaa M, Hillamo R, Brunekreef B, Katsouyanni K, et al. Dose and time dependency of inflammatory responses in the mouse lung to urban air coarse, fine, and ultrafine particles from six European cities. Inhal Toxicol. 2007;19:227–46.
49. Brook RD, Rajagopalan S, Pope CA, 3rd, Brook JR, Bhatnagar A, Diez-Roux AV, Holguin F, Hong Y, Luepker RV, et al. Particulate matter air pollution and cardiovascular disease: An update to the scientific statement from the American Heart Association. Circulation. 2010;121:2331–78.
50. Orellano P, Reynoso J, Quaranta N, Bardach A, Ciapponi A. Short-term exposure to particulate matter (PM10 and PM2.5), nitrogen dioxide (NO2), and ozone (O3) and all-cause and cause-specific mortality: Systematic review and meta-analysis. Environ Int. 2020;142: 105876.
51. Yue W, Tong L, Liu X, Weng X, Chen X, Wang D, Dudley SC, Weir EK, Ding W, Lu Z, et al. Short term Pm2.5 exposure caused a robust lung inflammation, vascular remodeling, and exacerbated transition from left ventricular failure to right ventricular hypertrophy. Redox Biol. 2019;22:101161.
52. Poh WJ, Wee CP, Gao Z. DNA Methyltransferase Activity Assays: Advances and Challenges. Theranostics. 2016;6:369–91.

53. Liao J, Karnik R, Gu H, Ziller MJ, Clement K, Tsankov AM, Akopian V, Gifford CA, Donaghey J, Galonska C, et al. Targeted disruption of DNMT1, DNMT3A and DNMT3B in human embryonic stem cells. Nat Genet. 2015;47:469–78.
54. Seelan RS, Mukhopadhyay P, Pisano MM, Greene RM. Effects of 5-Aza-2'-deoxycytidine (decitabine) on gene expression. Drug Metab Rev. 2018;50:193–207.
55. Christman JK. 5-Azacytidine and 5-aza-2'-deoxycytidine as inhibitors of DNA methylation: mechanistic studies and their implications for cancer therapy. Oncogene. 2002;21: 5483–95.
56. Naso MF, Tomkowicz B, Perry WL, 3rd, and Strohl WR. Adeno-Associated Virus (AAV) as a Vector for Gene Therapy. BioDrugs. 2017;31:317–334.
57. Wang H, Peng X, Cao F, Wang Y, Shi H, Lin S, Zhong W, Sun J. Cardiotoxicity and Mechanism of Particulate Matter 2.5 (PM2.5) Exposure in Offspring Rats During Pregnancy. Med Sci Monit. 2017;23:3890–3896.
58. Hu Q, Zhang H, Gutierrez Cortes N, Wu D, Wang P, Zhang J, Mattison JA, Smith E, Bettcher L. F, Wang M, Lakatta EG, Sheu SS, Wang W. Increased Drp1 Acetylation by Lipid Overload Induces Cardiomyocyte Death and Heart Dysfunction. Circ Res. 2020;126:456–470.
59. Sun Z, Zhang L, Li L, Shao C, Liu J, Zhou M,Wang Z. Galectin-3 mediates cardiac remodeling caused by impaired glucose and lipid metabolism through inhibiting two pathways of activating Akt. Am J Physiol Heart Circ Physiol. 2021;320:H364-H380.
60. Casquel De Tomasi L, Salome Campos DH, Grippa Sant'ana P, Okoshi K, Padovani CR, Masahiro Murata G, Nguyen S, Kolwicz SC, Jr., Cicogna AC. Pathological hypertrophy and cardiac dysfunction are linked to aberrant endogenous unsaturated fatty acid metabolism. PLoS One. 2018;13:e0193553.
61. Fieno DS, Hillenbrand HB, Rehwald WG, Harris KR, Decker RS, Parker MA, Klocke FJ, Kim RJ, Judd RM. Infarct resorption, compensatory hypertrophy, and differing patterns of ventricular remodeling following myocardial infarctions of varying size. J Am Coll Cardiol. 2004;43:2124–31.
62. Liang Q, De Windt LJ, Witt SA, Kimball TR, Markham BE, and Molkentin JD. The transcription factors GATA4 and GATA6 regulate cardiomyocyte hypertrophy in vitro and in vivo. J Biol Chem. 2001;276:30245–53.
63. Bai L, Zhao Y, Zhao L, Zhang M, Cai Z, Yung KKL, Dong C, Li R. Ambient air PM2.5 exposure induces heart injury and cardiac hypertrophy in rats through regulation of miR-208a/b, alpha/beta-MHC, and GATA4. Environ Toxicol Pharmacol. 2021;85:103653.
64. Onal G, Kutlu O, Gozuacik D, Dokmeci Emre S. Lipid Droplets in Health and Disease. Lipids Health Dis. 2017;16:128.
65. Herman-Edelstein M, Scherzer P, Tobar A, Levi M, Gafter U. Altered renal lipid metabolism and renal lipid accumulation in human diabetic nephropathy. J Lipid Res. 2014;55:561–72.
66. Bae H, Hong KY, Lee CK, Jang C, Lee SJ, Choe K, Offermanns S, He Y, Lee HJ, Koh GY. Angiopoietin-2-integrin alpha5beta1 signaling enhances vascular fatty acid transport and prevents ectopic lipid-induced insulin resistance. Nat Commun. 2020;11:2980.

67. Wang B, Tontonoz P. Phospholipid Remodeling in Physiology and Disease. Annu Rev Physiol. 2019;81:165–188.
68. Chen B, Sun Y, Niu J, Jarugumilli GK, Wu X. Protein Lipidation in Cell Signaling and Diseases: Function, Regulation, and Therapeutic Opportunities. Cell Chem Biol. 2018;25:817–831.
69. Fan J, Donkin J, Wellington C. Greasing the wheels of Abeta clearance in Alzheimer's disease: the role of lipids and apolipoprotein E. Biofactors. 2009;35:239–48.
70. Kolter T. Lipids and lipidomics. Angew Chem Int Ed Engl. 2006;45:5910–1.
71. Asakawa M, Takano H, Nagai T, Uozumi H, Hasegawa H, Kubota N, Saito T, Masuda Y, Kadowaki T, Komuro I. Peroxisome proliferator-activated receptor gamma plays a critical role in inhibition of cardiac hypertrophy in vitro and in vivo. Circulation. 2002;105:1240–6.
72. Xu Y, Gen M, Lu L, Fox J, Weiss SO, Brown RD, Perlov D, Ahmad H, Zhu P, Greyson C, et al. PPAR-gamma activation fails to provide myocardial protection in ischemia and reperfusion in pigs. Am J Physiol Heart Circ Physiol. 2005;288:H1314-23.
73. Armoni M, Harel C, Karni S, Chen H, Bar-Yoseph F, Ver MR, Quon MJ, Karnieli E. FOXO1 represses peroxisome proliferator-activated receptor-gamma1 and -gamma2 gene promoters in primary adipocytes. A novel paradigm to increase insulin sensitivity. J Biol Chem. 2006;281:19881–91.
74. Khuchua Z, Glukhov AI, Strauss AW, Javadov S. Elucidating the Beneficial Role of PPAR Agonists in Cardiac Diseases. Int J Mol Sci. 2018;19.
75. Oka S, Alcendor R, Zhai P, Park JY, Shao D, Cho J, Yamamoto T, Tian B, Sadoshima J. PPARalpha-Sirt1 complex mediates cardiac hypertrophy and failure through suppression of the ERR transcriptional pathway. Cell Metab. 2019;14:598–611.
76. Madsen A, Hoppner G, Krause J, Hirt MN, Laufer SD, Schweizer M, Tan WLW, Mosqueira D, Anene-Nzelu CG, Lim I, Foo RSY, et al. An Important Role for DNMT3A-Mediated DNA Methylation in Cardiomyocyte Metabolism and Contractility. Circulation. 2020;142:1562–1578.
77. Carrasco S, Merida I. Diacylglycerol, when simplicity becomes complex. Trends Biochem Sci. 2007;32:27–36.
78. Castro B. M, Prieto M, Silva LC. Ceramide: a simple sphingolipid with unique biophysical properties. Prog Lipid Res. 2014;54:53–67.
79. Kim SC, Wang X. Phosphatidic acid: an emerging versatile class of cellular mediators. Essays Biochem. 2020;64:533–546.
80. Mohamed A, Molendijk J, Hill MM. lipidr: A Software Tool for Data Mining and Analysis of Lipidomics Datasets. J Proteome Res. 2020;19:2890–2897.
81. Huynh K, Lim WLF, Giles C, Jayawardana KS, Salim A, Mellett NA, Smith AAT, Olshansky G, Drew BG, Chatterjee P, et al. Concordant peripheral lipidome signatures in two large clinical studies of Alzheimer's disease. Nat Commun. 2020;11:5698.
82. Xu T, Hu C, Xuan Q, Xu G. Recent advances in analytical strategies for mass spectrometry-based lipidomics. Anal Chim Acta. 2020;1137:156–169.

Tables

Table 1. PCR primer design summary.

Gene	Primer sequence (5’-3’)	Length (bp)
PDGFRβ	F:GTCAAGATGCTGAAATCGACAG	22
	R:GGGGTCCAAGATGACTCATAAT	22
RAS	F:GCATCCCCTACATTGAAACATC	22
	R:CAATTTATGCTGCCGAATCTCA	22
RAF	F:AGGCAGGAGAAAGGCGAGAGG	21
	R:AAGGACCGAGCACAGGAAGAGG	22
MEK	F:AAAAGAGAAGGTGAAGAAGGGC	22
	R:CAAATTCCTTCTTCCAGTTGCA	22
ERK	F:ATCTCAACAAAGTTCGAGTTGC	22
	R:GTCTGAAGCGCAGTAAGATTTT	22
GAPDH	F:CGTGCCGCCTGGAGAAACCTG	21
	R:AGAGTGGGAGTTGCTGTTGAAGTCG	25
DNMT1	F:GAGACGAAAAACGACACGTAAA	22
	R:CACTTTGGTGAGTTGATCTTCG	22
DNMT3A	F:GATGATCGAAAGGAAGGAGAGG	22
	R:TTCTCCAAGTCTCCATTGGGTA	22
DNMT3B	F:GCTCTTCTTCGAGTTTTACCAC	22
	R:ATCATTCTTTGAAGCCATCACG	22
ANF	F:GGTCTAGTGGGGTCTTGCCTCTC	23
	R:GCGTCTGTCCTTGGTGCTGAAG	22
BNF	F:TGCTGGAGCTGATAAGAGAAAA	22
	R:GAAGGACTCTTTTTGGGTGTTC	22
β-MHC	F:TTCGCCCTTTGTTCCCATTGTCTC	24
	R:GGTTGACGGTGACGCAGAAGAG	22

Figures

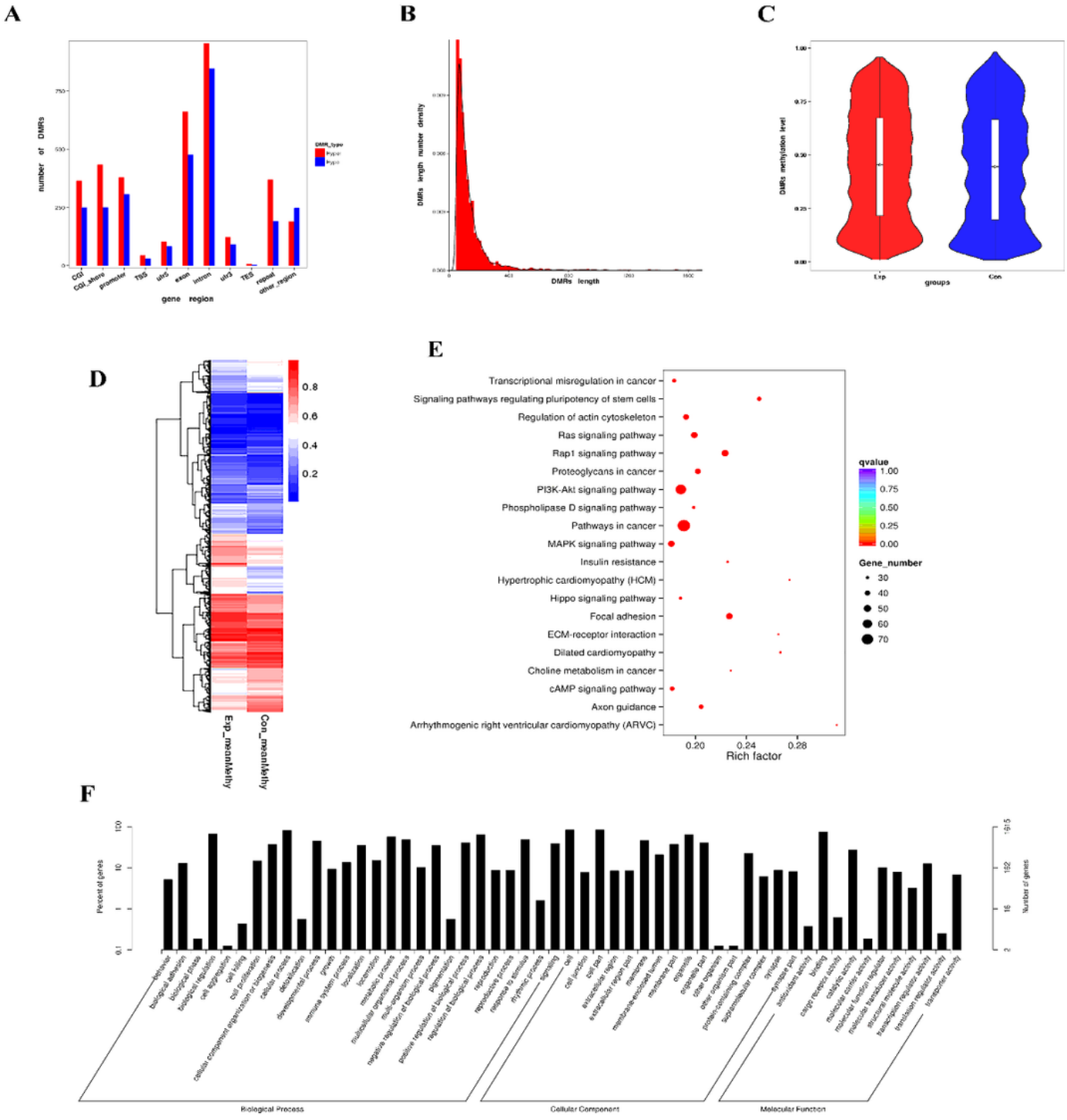

Figure 1

Reduced representation bisulfite sequencing was performed on C57BL/6J mice. Mice were exposed to ambient PM for 42 days in a individual ventilated cage based system. a For DMR anchor regions (such as Promoter, Exon, Intron, CGI, CGI Shore, Repeat, TSS, TES, etc.), statistical mapping was performed to differentiate Hyper (hypermethylated DMR) and Hypo (hypmethylated DMR). The horizontal axis represents each region category, and the vertical axis represents the number of Hyper/Hypo DMR in each

region; b CG sequence environment DMR length display mapping. The abscissa represents the DMR length, the ordinate represents the density value at each length, and the black represents the distribution fitting curve; c Plot violin boxplot for DMR methylation level. The horizontal coordinate represents the comparison group, and the vertical coordinate represents the methylation level value. The distribution of the methylation level of DMR is shown in the form of a violin plot (boxplot inside, and the number distribution at this methylation level on the side); d CG sequence environment DMR methylation level clustering heat map. Abscissa represents comparison group, ordinate represents clustering effect of methylation level value, blue to red represents from low to high methylation level.; e scatter diagram of KEGG metabolic pathway enrichment. The ordinate represents pathway name, the abscissa represents Rich factor, the size of dots indicates the number of DMR-related genes in this pathway, and the color of dots corresponds to different Qvalue ranges; f GO grading annotation map for all DMR genes. The ordinate is the percentage of the number of DMR related genes, and the ordinate is the enriched GO term.

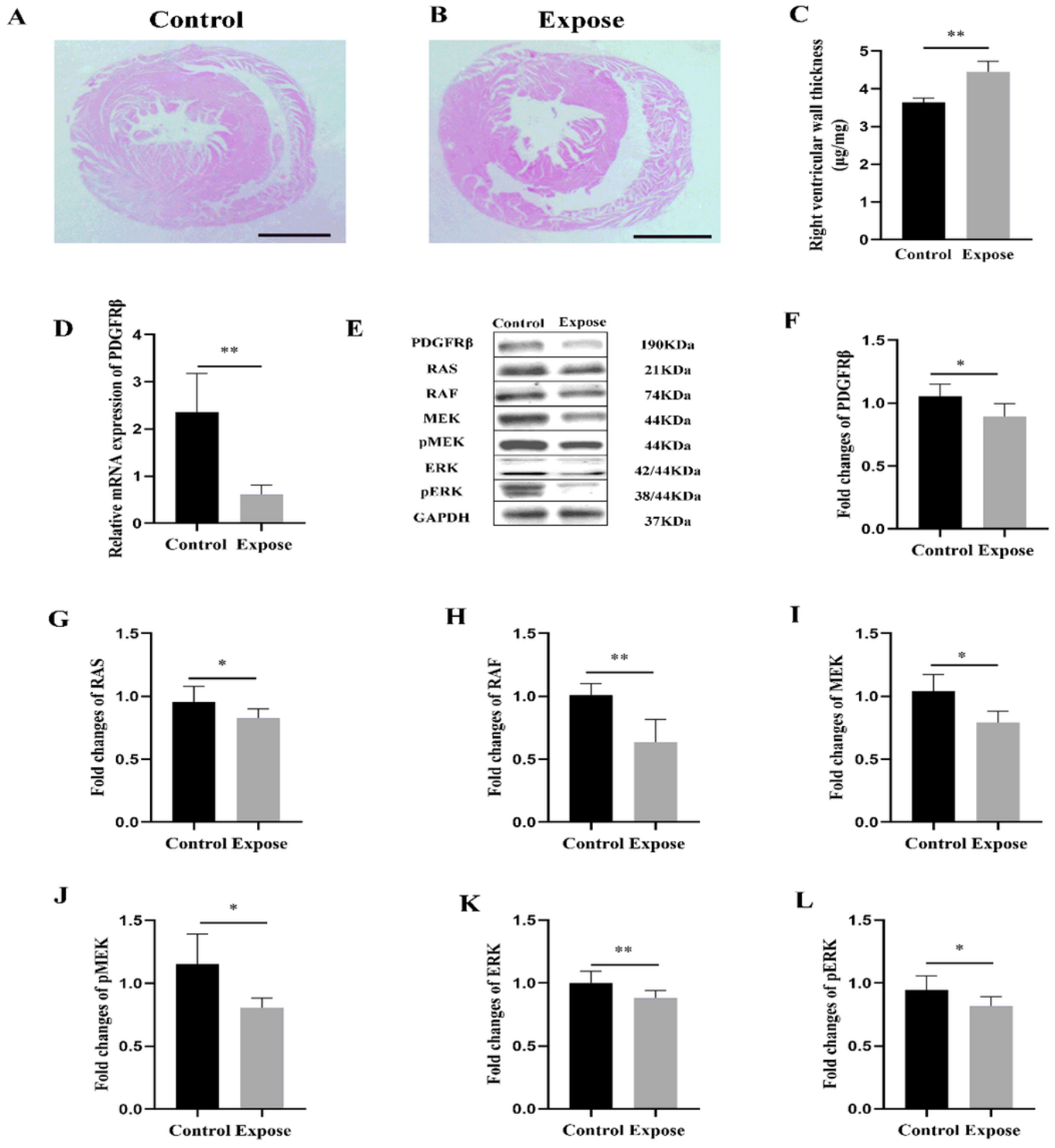

Figure 2

PM induces PDGFRβ hypermethylation and cardiac hypertrophy through the MEK/ERK pathway of C57BL/6J mice in the real-ambient PM exposure system. a-b Morphological evaluation of the heart in treated animals at 42 days. C57BL/6J C57BL/6Jmice were reared in an independent ventilation cage (IVC) system for 6 weeks and then sacrificed. Right ventricular wall thickness was measured and normalized to whole heart weight. Control: Representative micrograph of heart tissue of control animals.

Exposure: Representative microscopic image of animal heart tissue exposed only to PM; c Quantification of the right ventricular wall thickness; d RT-qPCR analysis of PDGFRβ in mouse hearts 42 days after real-ambient PM exposure; e Western blot results showed that the expression of related proteins in the MEK/ERK pathway changed significantly after 42 days of PM exposure compared with the control group; f Relative protein expression of PDGFRβ; g Relative protein expression of RAS; h Relative protein expression of RAF; i Relative protein expression of MEK; j Relative protein expression of pmek; k Relative protein expression of ERK; l Relative protein expression of pERK. *: Statistically different from control animals ($P < 0.05$).

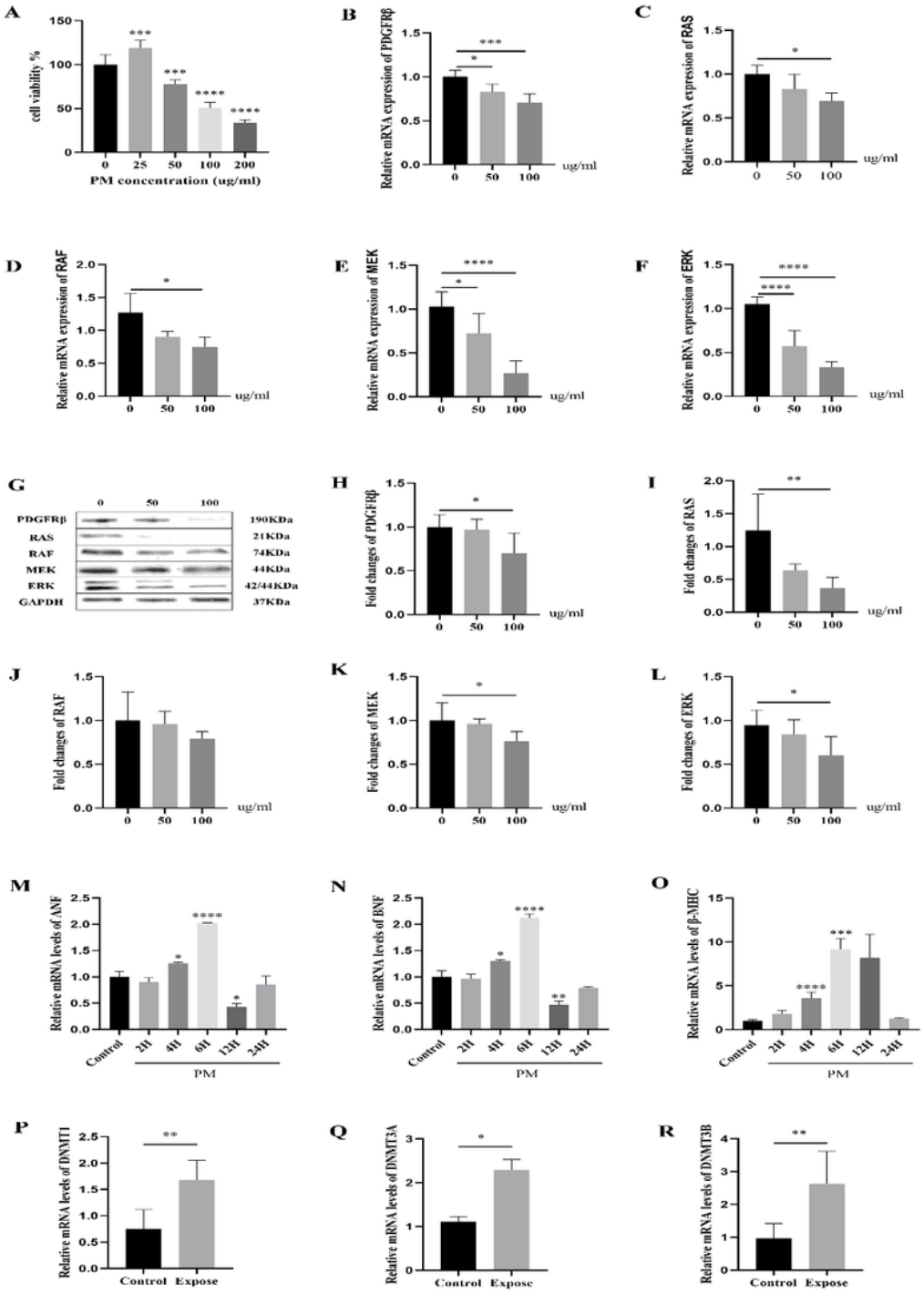

Figure 3

Effect of PM at different concentrations and at different times on MEK/ERK pathway and myocardial hypertrophy. a Cell viability of primary neonatal rat cardiomyocytes was measured by CCK8 method after exposure to PM at different concentrations (0, 25, 50, 100, 200 μg/ mL) for 24 hours; b RT-qPCR analysis of PDGFRβ in primary neonatal rat cardiomyocytes exposed to different PM concentrations (0, 50, 100 μg/mL) for 24 hours; c RT-qPCR analysis of RAS in primary neonatal rat cardiomyocytes after 24 hours

exposure at different PM concentrations (0, 50, 100 μg/mL); d RT-qPCR analysis of RAF in primary neonatal rat cardiomyocytes after 24 hours exposure at different PM concentrations (0, 50, 100 μg/ mL); e RT-qPCR analysis of MEK in primary neonatal rat cardiomyocytes after 24 h exposure at different PM concentrations (0, 50, 100 μg/mL); f RT-qPCR analysis of ERK in primary neonatal rat cardiomyocytes after 24 h exposure at different PM concentrations (0, 50, 100 μg/mL); g Western blot analysis showed that compared with the control group, the protein expression of primary neonatal rat cardiomyocytes was significantly changed after different doses of PM (0, 50, 100 μg/mL); h Relative protein expression of PDGFRβ compared with the control group; i Relative protein expression of RAS; j Relative protein expression of RAF; k Relative protein expression of MEK; l Relative protein expression of ERK. 50 μg/mL had relatively low cytotoxicity for the next experiment; m Different time points (0, 2 4 6, 12 and 24 hours) RT-qPCR analysis of ANF in primary neonatal rat cardiomyocytes; n Different time points (0, 2 4 6, 12 and 24 hours) RT-qPCR analysis of BNF in primary neonatal rat cardiomyocytes; o Different time points (0, 2 4 6, 12 and 24 h) RT-qPCR analysis of β-MHC in primary neonatal rat cardiomyocytes. PM exposure 6H was selected for the next experiment; p The concentration of PM was 50 μg/mL and the exposure time was 6 hours for RT-qPCR analysis of DNMT1 in primary neonatal rat cardiomyocytes; q The concentration of PM was 50 μg/mL and the exposure time was 6 hours for RT-qPCR analysis of DNMT3A in primary neonatal rat cardiomyocytes; r The concentration of PM was 50 μg mL and the exposure time was 6 hours for RT-qPCR analysis of DNMT3B in primary neonatal rat cardiomyocytes. *:P<0.05. * *: P<0.01.* * *: P<0.001. * * * *: P<0.0001.

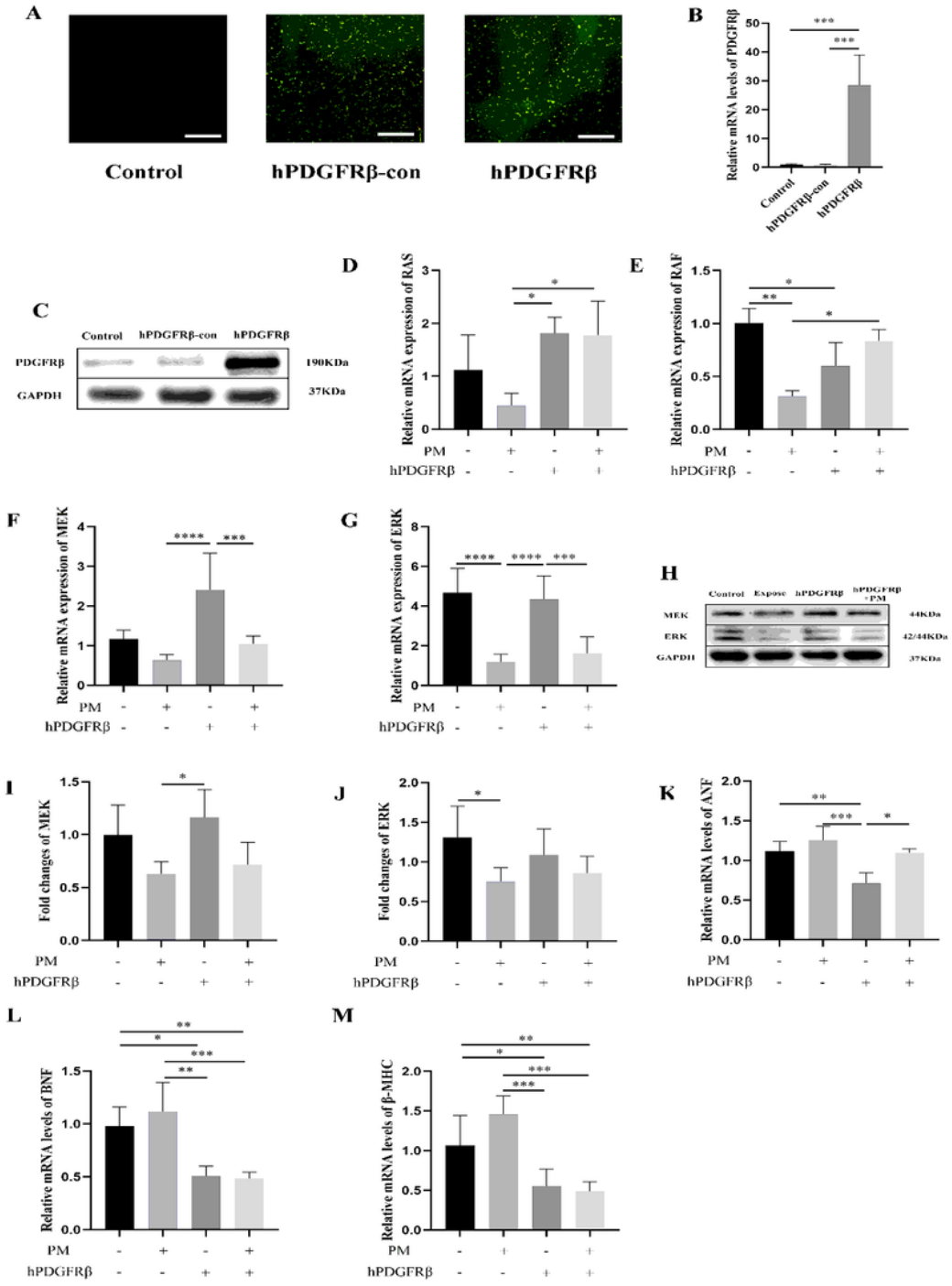

Figure 4

hPDGFβ and RT-qPCR and WB analysis of related genes in MEK/ERK pathway were performed in the transfected primary neonatal rat cardiomyocytes mice treated with PM. a Fluorescence image showing transfection efficiency of primary myocardial cells (magnification, 10x). hPDGFRβ-con represents cells transfected with empty plasmids, and hPDGFRβ represents cells transfected with PDGFRβ overexpressed recombinant plasmids; b RT-qPCR analysis of PDGFRβ mRNA expression after transfection with

recombinant plasmid; c Western blot analysis of PDGFRβ protein expression after transfection with recombinant plasmid. d-g RT-qPCR analysis of relative mRNA expression of RAS, RAF, MEK, ERK in primary myocardial cells after transfection with recombinant plasmid and/or PM exposure; h Western blot analysis highlighted significant changes in hPDGFRβ protein expression after transfection of primary myocardial cells with hPDGFRβ plasmid and/or PM treatment; i Relative protein expression of MEK; j Relative protein expression of ERK; k RT-qPCR analysis of relative mRNA expression of ANF after recombinant plasmid transfection and/or PM exposure in primary myocardial cells; l RT-qPCR analysis of BNF relative mRNA expression after recombinant plasmid transfection and/or PM exposure in primary myocardial cells; m RT-qPCR analysis of relative mRNA expression of β-MHC after recombinant plasmid transfection and/or PM exposure in primary myocardial cellsv. *: $P < 0.05$. * *: $P < 0.01$. * * *: $P < 0.001$. * * * *: $P < 0.0001$.

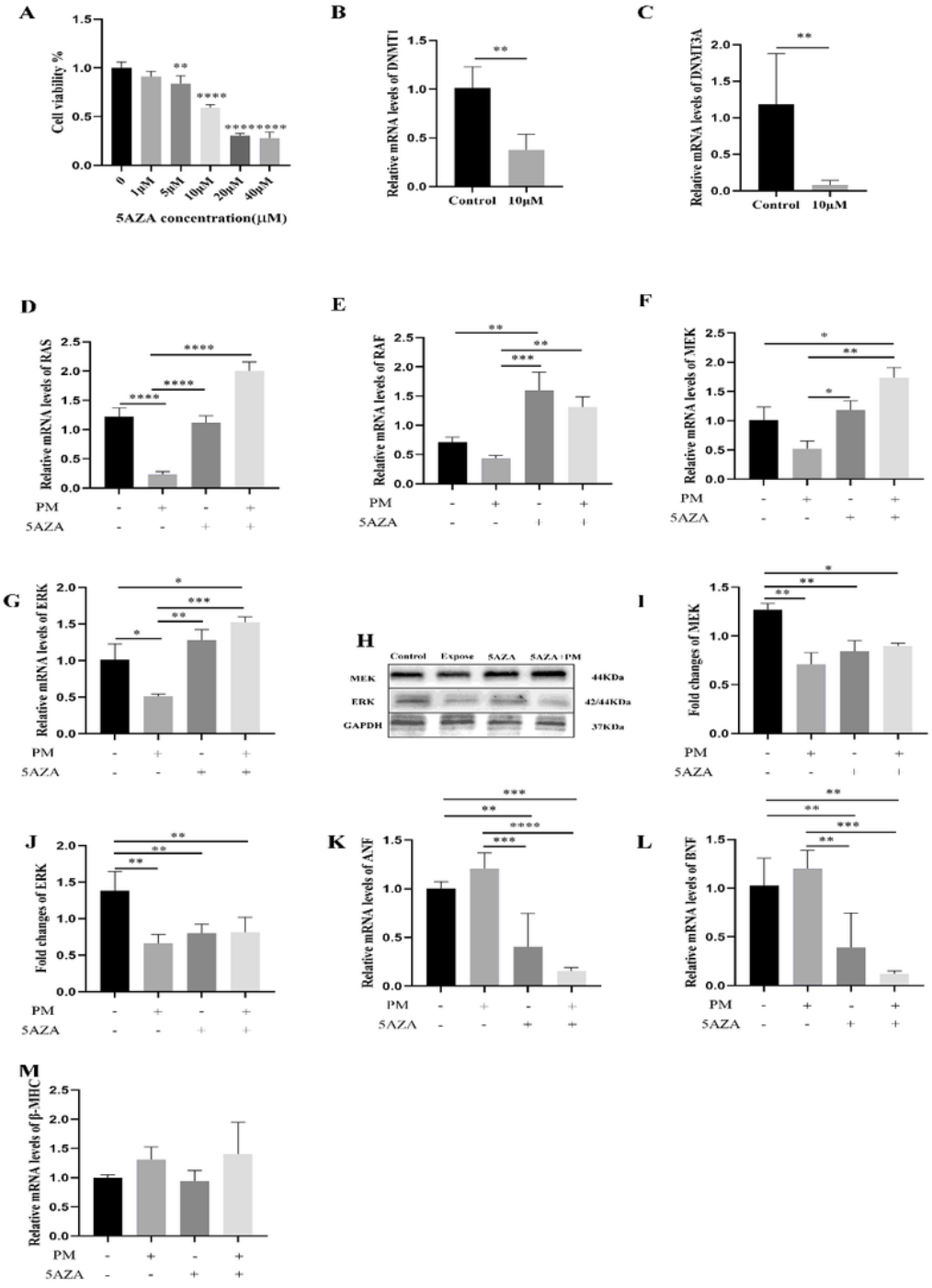

Figure 5

RT-qPCR and WB analysis of related genes in MEK/ERK pathway after PM treatment and methylated suppressed in primary neonatal rat cardiomyocytes rat. a cell viability of primary neonatal rat cardiomyocytes was measured by CCK8 method after 24 hours exposure to different methylation inhibitor concentrations of 5-AZA (0, 1, 5, 10, 20, 40 μM). 10 μg/mL displayed relatively low cytotoxicity and was used for the next experiments; b RT-qPCR analysis of DNMT1 in primary myocardial cells at a

methylation inhibitor concentration of 10 μM; c RT-qPCR analysis of DNMT3A in primary myocardial cells at a methylation inhibitor concentration of 10 μM; d-g RT-qPCR analysis of relative mRNA expression of RAS, RAF, MEK, ERK after exposure to methylation inhibitor 5AZA and/or PM in primary myocardial cells; h Western blot results showed significant changes in protein expression after treatment with the primary myocardial cells methylation inhibitor 5AZA and/or PM exposure. i Relative protein expression of MEK; j Relative protein expression of ERK; k RT-qPCR analysis of relative mRNA expression of ANF after treatment with methylation inhibitor 5AZA and/or PM exposure in primary myocardial cells; l RT-qPCR analysis of BNF relative mRNA expression after treatment with methylation inhibitor 5AZA and/or PM exposure in primary myocardial cells; m RT-qPCR analysis of β-MHC relative mRNA expression after methylation inhibitor 5AZA treatment and/or PM exposure in primary cardiomyocytes. *: $P < 0.05$. * *: $P < 0.01$. * * *: $P < 0.001$. * * * *: $P < 0.0001$.

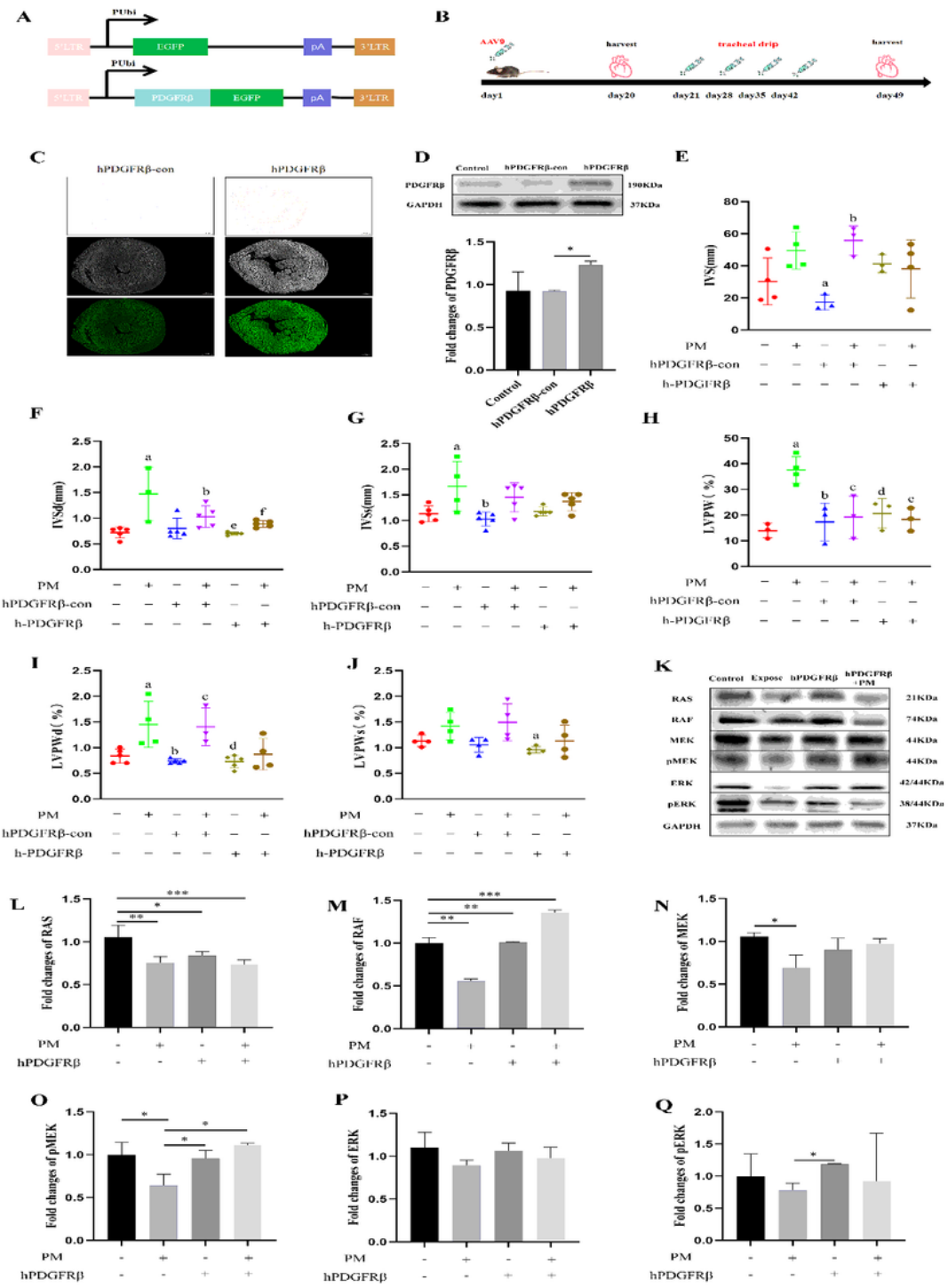

Figure 6

hPDGFRβ mitigated myocardial hypertrophic by PM exposure through the MEK/ERK pathway in C57BL/6J mice. a AAV9: hPDGFRβ-con and AAV9: hPDGFRβ were generated using AAV vectors, which contain AAV reverse terminal repeat sequence (ITRs), promoter (PUbi) and polyadenylation (pA); b Schematic diagram of PM tracheal drip. model after tail vein injection of AAV9. 20 days after AAV9 injection, the high expression model of PDGFRβ was observed and tracheal infusion was performed once

a week for a month; c immunohistochemical staining and fluorescence images of the mouse heart after AAV920 days of tail vein injection; d Western blot results showed PDGFRβ expression after AAV9 20 days of tail vein administration; e Quantitative results of IVS in ultrasound electrocardiogram. a: The difference between PM group and hPDGFRβ -con group was statistically significant, P<0.05. b: The difference between hPDGFRβ -con group and hPDGFRβ -con +PM group was statistically significant, P<0.05; f Quantitative results of IVSd in ultrasound electrocardiogram. a: The difference between the control group and the PM exposure group was statistically significant, P<0.001. b: The difference between PM exposure group and hPDGFRβ-con group was statistically significant, P<0.01. c: PM exposure group and hPDGFRβ group, the difference was statistically significant, P<0.001. d: The difference between PM exposure group and hPDGFRβ+PM group was statistically significant, P<0.05; g Quantitative results of IVSs in ultrasound electrocardiogram. a: The difference between the control group and PM exposure group was statistically significant, P<0.05. b: The difference between PM exposure group and hPDGFRβ-con group was statistically significant, P<0.01; h Quantitative results of LVPW in echocardiogram. a: The difference between the control group and the PM exposure group was statistically significant, P<0.01. b: The difference between PM exposure group and hPDGFRβ-con group was statistically significant, P<0.01. c: PM group and hPDGFRβ-con group, the difference was statistically significant, P<0.05. d: PM group and PDGFRβ-con group, the difference was statistically significant, P<0.05. e: The difference between PM exposure group and hPDGFRβ+PM group was statistically significant, P<0.01; i Quantitative results of LVPWd in echocardiogram. a: The difference between the control group and PM exposure group was statistically significant, P<0.05. b: The difference between PM exposure group and hPDGFRβ-con group was statistically significant, P<0.01. c: PM group and hPDGFRβ group, the difference was statistically significant, P<0.01. d: The difference between PM exposure group and hPDGFRβ+PM group was statistically significant, P<0.05; j Quantitative results of LVPWs in echocardiogram. a: hPDGFRβ-con+PM and hPDGFRβ group, the difference was statistically significant, P<0.05. k Western blot results showed that protein expression of AAV9 in C57BL/6J mice was significantly changed after tail vein injection and/or tracheal drip of PM. l Relative protein expression of RAS; m Relative protein expression of RAF; n Relative protein expression of MEK; o Relative protein expression of pMEK; p Relative protein expression of ERK; q Relative protein expression of pERK. *: P < 0.05. * *: P < 0.01. * * *: P < 0.001. * * * *: P < 0.0001.

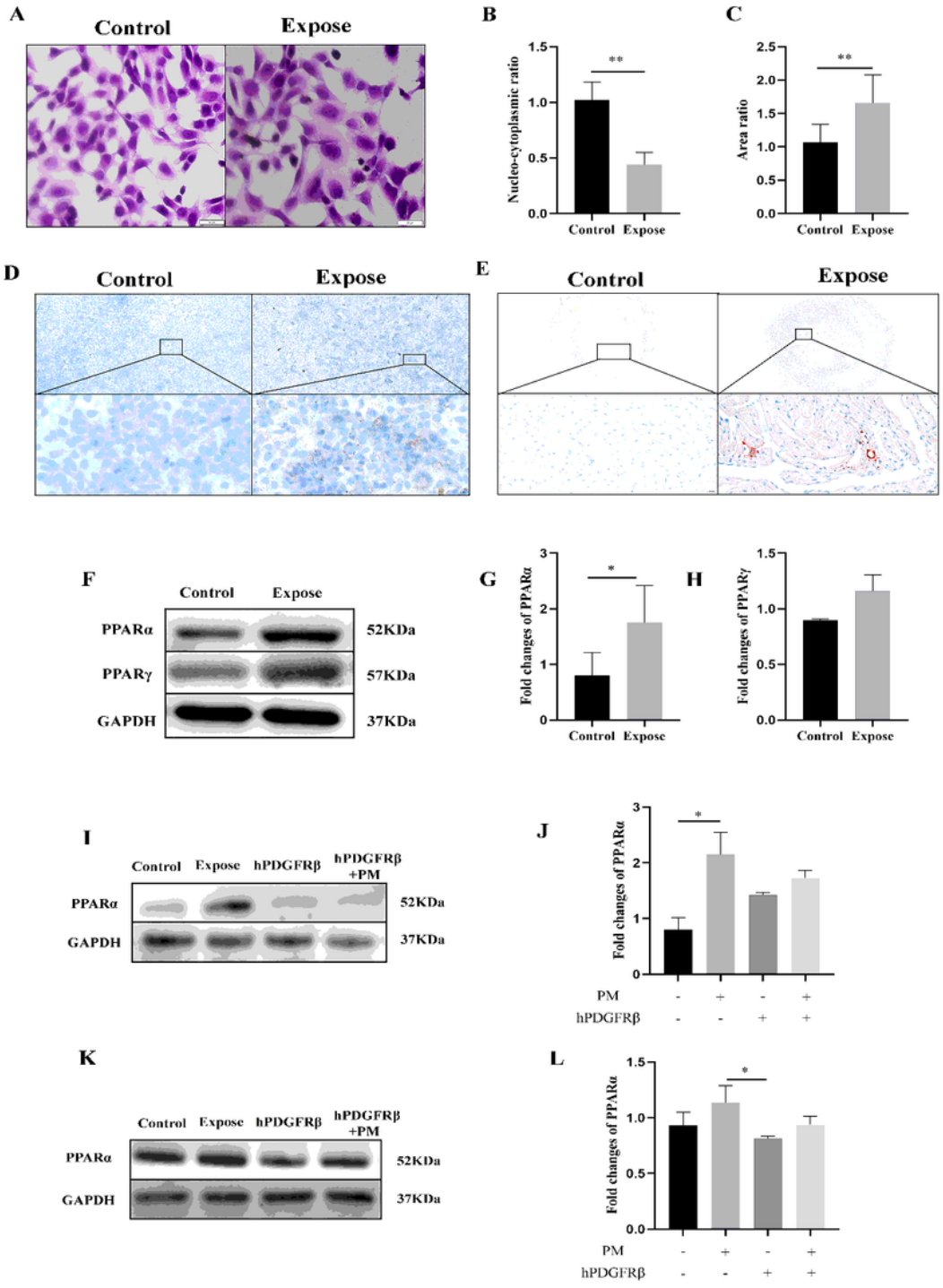

Figure 7

hPDGFRβ ameliorates the effects of PM exposure on myocardial hypertrophy and myocardial lipid metabolism disorders in AC16 cells. a AC16 cells were stained with hematoxylin and eosin in the control and PM exposed groups. (Magnification, 40x); b Nucleo-plasmic ratio was expressed in AC16 cells in the control and PM exposed groups; c the area ratio of AC16 cells in the control group and PM exposed group was relative; d Oil red O staining of AC16 cells in control group and PM exposed group. The lower panels

are high magnification (40×) images corresponding to the upper panels (5×); e The heart tissue of C57BL/6J mice was stained with oil red O in the control group and PM exposed group. The blow panels are high magnification (40×) images corresponding to the upper panels (5×); f PPARα and PPARγ changed significantly one month after PM tracheal drip compared with the control group; g Relative protein expression of PPARα; h Relative protein expression of PPARγ; i Western blot results showed that AC16 cells were significantly altered after transfection with hPDGFRβ plasmid and/or PM treatment; j Relative protein expression of PPARα in AC16 cells; k Western blot results showed significant changes in protein expression after tail vein administration of AAV9 and/or PM treatment in C57 /B6 mice; l Relative protein expression of PPARα in C57 /B6 mice.*:P<0.05.**:P<0.01.***:P<0.001.****:P<0.0001.

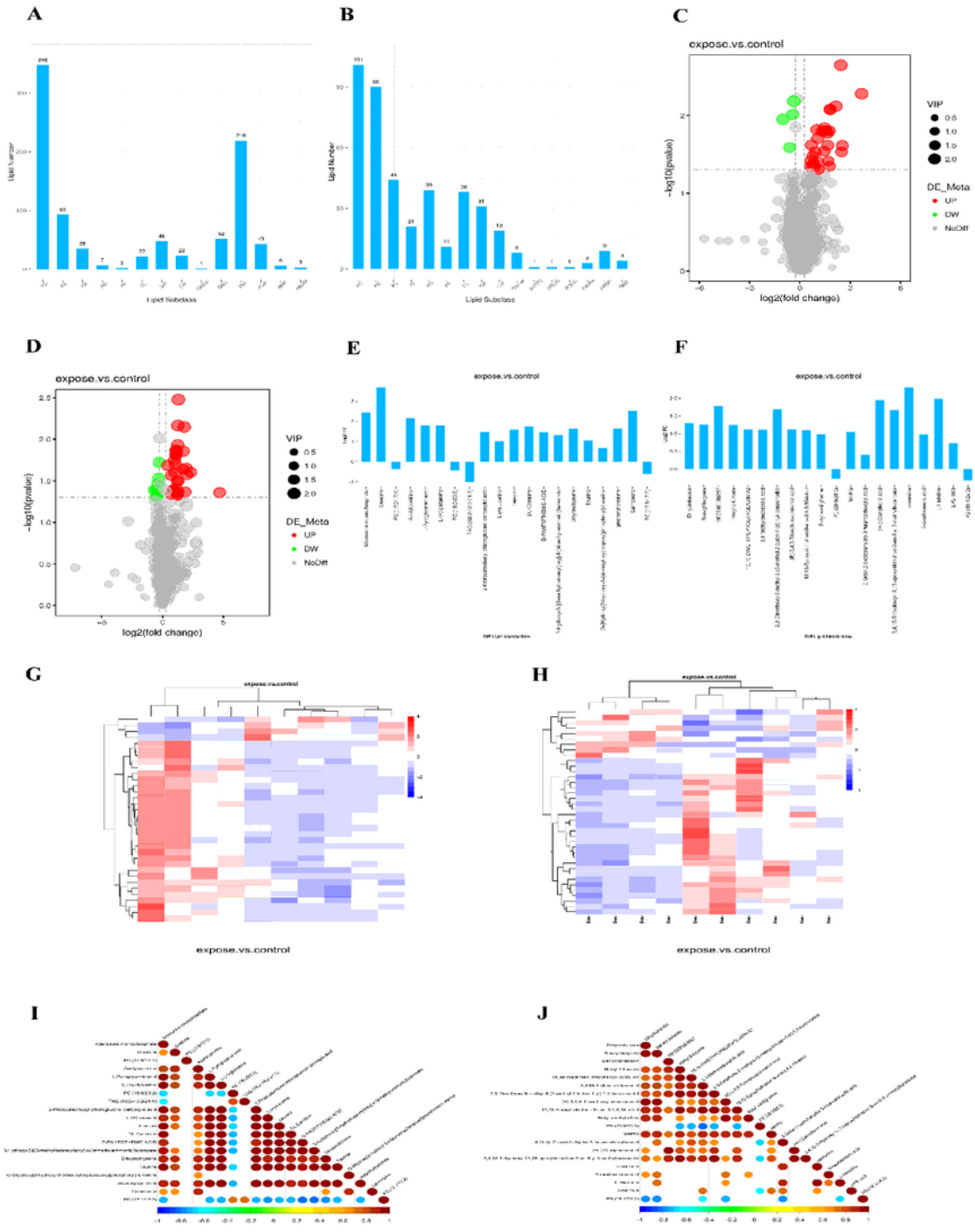

Figure 8

Lipidomic analysis of PM control group and PM exposure group in C57BL/6J mice. a Lipid subclass analysis in positive ion mode. Longitudinal is the number of lipid compounds contained in each lipid subclass, and transverse is each lipid subclass; b Lipid subclass analysis in anion mode. Longitudinal is the number of lipid compounds contained in each lipid subclass, and transverse is each lipid subclass; c Volcano plot of differential lipid compounds in positive ion mode. The horizontal axis represents the

change of expression multiple of lipid compounds in different groups (Log2(Fold Change)), and the vertical axis represents the significance level of difference (-log10(P_value)). Each point in the volcano plot represents a lipid compound. Significantly up-regulated lipids are represented by red dots, significantly down-regulated lipids are represented by green dots, and the size of the dots represents VIP values; d Volcano diagram of differential lipid compounds in negative ion mode, the horizontal axis represents the change of expression multiple of lipid compounds in different groups log2(Fold Change)), and the vertical axis represents the significance level of difference (-log10(P value)). Each point in the volcano diagram represents a lipid compound. Significantly up-regulated lipids are represented by red dots, significantly down-regulated lipids are represented by green dots, and the size of the dots represents VIP values; e Differential multiple analysis diagram of differential lipid compounds in positive ion mode. The vertical diagram shows log2(Fold change) values of differential lipid compounds, and the horizontal diagram shows the log2(Fold change) values of the top 20 differential lipid compounds in each comparison pair from small to large; f Differential multiple analysis diagram of differential lipid compounds in negative ion mode, the vertical is the log2(Fold change) value of differential lipid compounds, and the horizontal is the log2(Fold change) value of the top 20 differential lipid compounds in each comparison pair, and the Fig shows the log2(Fold change) value of the top 20 differential lipid compounds according to p-value from small to large; g Cluster analysis diagram of differential lipid compounds in positive ion mode. Longitudinal is the cluster of samples, and transverse is the cluster of metabolites. The shorter the cluster branch, the higher the similarity. The relationship of metabolite content clustering between groups can be seen by horizontal comparison; h Cluster analysis diagram of differential lipid compounds in negative ion mode. Longitudinal is the cluster of samples, and transverse is the cluster of metabolites. The shorter the cluster branch, the higher the similarity. The relationship of metabolite content clustering between groups can be seen by horizontal comparison; i Correlation analysis diagram of differential lipid compounds in positive ion mode, with the highest correlation of 1 and a complete positive correlation (red), and the lowest correlation of -1 and a complete negative correlation (blue). The part without color represents p-value > 0.05. The Fig shows the correlation of the top 20 different lipid compounds in order of p-value from small to large; j Correlation analysis diagram of differential lipid compounds in negative ion mode, the highest correlation is 1, indicating a complete positive correlation (red), and the lowest correlation is -1, indicating a complete negative correlation (blue). The part without color indicates p-value > 0.05. The Fig shows the correlation of the Top20 different lipid compounds in order of p-value from small to large.

Supplementary Files

This is a list of supplementary files associated with this preprint. Click to download.

- Onlinefloatimage1.png